National Park Service
U.S. Department of the Interior

Natural Resource Stewardship and Science

High-Resolution Permafrost Modeling in Wrangell-St. Elias National Park and Preserve

Natural Resource Technical Report NPS/CAKN/NRTR—2014/861

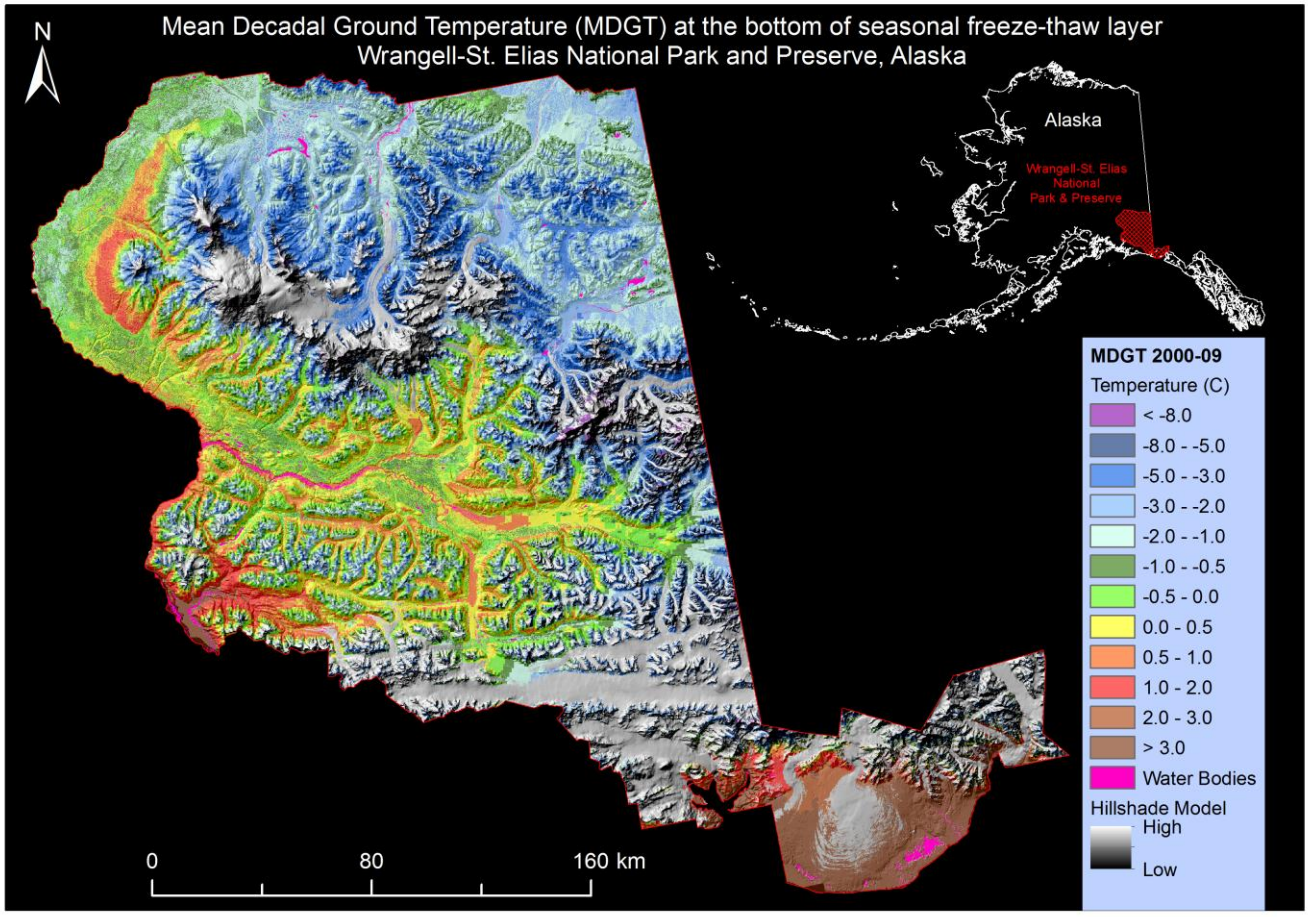

ON THE COVER

Permafrost map of Wrangell-St. Elias National Park and Preserve, Alaska. The negative temperature values, shown in shades of green and blue, indicate presence of near-surface permafrost. The positive temperature values, shown in shades of brown and red, indicate absence of near-surface permafrost. The acronym MDGT stands for Mean Decadal Ground Temperature. The MDGT map is draped over a hillshade model shown in grayscale. The hillshade model is apparent in places where glaciers are masked out.

Image courtesy of S. K. Panda.

High-Resolution Permafrost Modeling in Wrangell-St. Elias National Park and Preserve

Natural Resource Technical Report NPS/CAKN/NRTR—2014/861

Santosh K. Panda
Sergey S. Marchenko
Vladimir E. Romanovsky

Geophysical Institute
University of Alaska Fairbanks
903 Koyukuk Drive
Fairbanks, Alaska 99775

April 2014

U.S. Department of the Interior
National Park Service
Natural Resource Stewardship and Science
Fort Collins, Colorado

The National Park Service, Natural Resource Stewardship and Science office in Fort Collins, Colorado, publishes a range of reports that address natural resource topics. These reports are of interest and applicability to a broad audience in the National Park Service and others in natural resource management, including scientists, conservation and environmental constituencies, and the public.

The Natural Resource Technical Report Series is used to disseminate results of scientific studies in the physical, biological, and social sciences for both the advancement of science and the achievement of the National Park Service mission. The series provides contributors with a forum for displaying comprehensive data that are often deleted from journals because of page limitations.

All manuscripts in the series receive the appropriate level of peer review to ensure that the information is scientifically credible, technically accurate, appropriately written for the intended audience, and designed and published in a professional manner. This report received informal peer review by subject-matter experts who were not directly involved in the collection, analysis, or reporting of the data.

Views, statements, findings, conclusions, recommendations, and data in this report do not necessarily reflect views and policies of the National Park Service, U.S. Department of the Interior. Mention of trade names or commercial products does not constitute endorsement or recommendation for use by the U.S. Government.

This report is available in digital format from the Central Alaska Network http://science.nature.nps.gov/im/units/cakn/index.cfm and Natural Resource Publications Management website (http://www.nature.nps.gov/publications/nrpm/). To receive this report in a format optimized for screen readers, please email irma@nps.gov.

Please cite this publication as:

Panda, S. K., S. S. Marchenko, and V. E. Romanovsky. 2014. High-resolution permafrost modeling in Wrangell-St. Elias National Park and Preserve. Natural Resource Technical Report NPS/CAKN/NRTR—2014/861. National Park Service, Fort Collins, Colorado.

NPS 190/124322, April 2014

Contents

Contents (continued)

Figures

Page

Tables

Page

Executive Summary

We used the CRU (1950-1959 and 2000-2009) and projected 5-GCM composite (2001-2010, 2051-2060, and 2091-2100) decadal climate forcing, ecotype (Jorgenson et al. 2008), soil landscape (Jorgenson et al. 2008), and snow (unpublished) maps of WRST to model the presence or absence of near-surface permafrost, temperature at the bottom of seasonal freeze-thaw layer and thickness of seasonal freeze-thaw layer within WRST. We produced permafrost temperature and active-layer and seasonally-frozen-layer thickness distribution maps through this modeling effort at a pixel spacing of 28.5 m. This is an immense improvement over the spatial resolution of existing permafrost maps on any part of Alaska, whether produced through the spatially explicit thermal modeling of ground temperatures or by visual interpretation of satellite images/ aerial photos using indirect surface evidences of permafrost or by compilation of information from detailed field soil/ geology/ecotype surveys. The model predicted 'stable' near-surface permafrost under 72% of WRST total area during decade 2000s and its distribution is predicted to decline to—42% by 2050s and 15% by 2090s (Figure i). The accuracy tests of the modeled permafrost, and active-layer and seasonally-frozen-layer thickness maps by comparing them against the field observations of permafrost presence/absence (at 430 sites within WRST) suggested 91% agreement.

We compiled the available ground temperature data from three climate stations within WRST and compared them to the modeled ground temperatures (Table 3). We attributed the air temperature differences between climate stations and the CRU and 5-GCM composite data (input climate forcings) to the difference in scale of these datasets. The difference between recorded near-surface ground temperatures (at 0.05 m) and modeled ground surface temperatures were <1°C at Chicken Creek and ~2.0°C at Gates Glacier. We attributed these differences in temperatures to three major factors: difference in scale, ground condition, and snow depth.

The GIPL 1.0 model performs competently for WRST and provides reliable permafrost temperature status for different time-periods. As we used past and projected future climate forcing for modeling, the output permafrost maps show the impact of changing climate on near-surface permafrost temperature and its distribution. These permafrost maps will facilitate the park mangers to understand the current status of near-surface permafrost within WRST and how it may evolve in the future with changing climate, also to identify (vulnerable) sites at higher risk of permafrost thawing, with concurrent changes in wildlife habitats and populations. These maps will enable the park managers and decision makers to make informed decision on resource management and design of monitoring programs. Nonetheless, our model is limited in its ability to incorporate temporal changes in vegetation dynamics which could affect near-surface permafrost dynamics. Though we assumed no change in vegetation dynamics for our modeling time periods, the natural disturbances like forest fires and flooding could alter the vegetation structure and composition and consequently the ecotype at the disturbed sites resulting in reduced model prediction accuracy at those sites in the future.

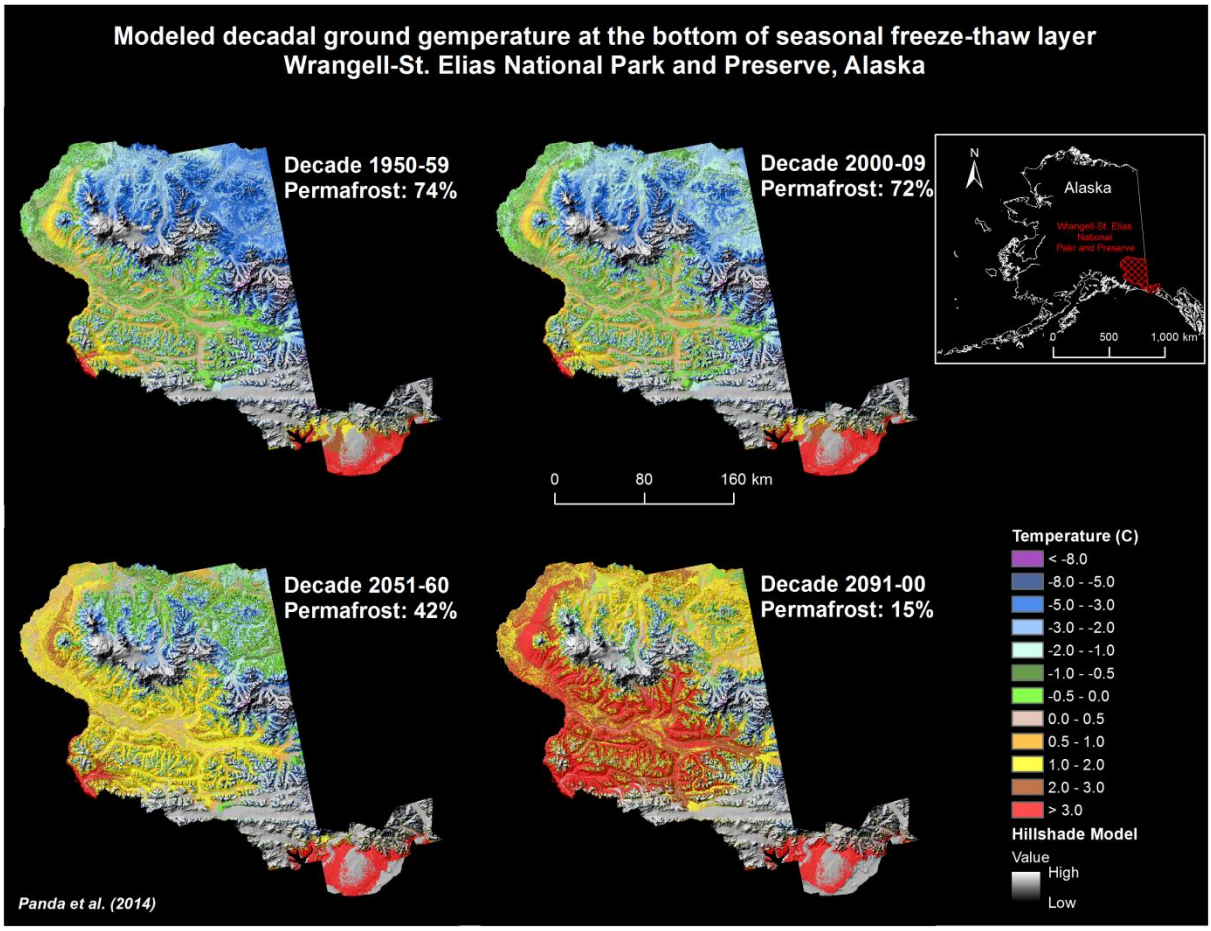

Figure i. Comparison of modeled permafrost maps (CRU forcing: 1950s and 2000s; 5-GCM forcing: 2050s and 2090s) of Wrangell-St. Elias National Park and Preserve. The negative temperature values, shown in shades of green and blue, indicate presence of near-surface permafrost. The positive temperature values, shown in shades of brown and red, indicate absence of near-surface permafrost. The permafrost maps are draped over hillshade model shown in gray scale. The hillshade model is apparent in places where glaciers and permanent ice-fields are masked out of the permafrost map.

Acknowledgments

We would like to offer our special thanks to David K Swanson for his valuable advice, support and overall management of this project. His enthusiasm for the project and willingness to give time generously has been very much appreciated. We would also like to thank Pam Sousanes for help in accessing National Park Service climate data.

List of Acronyms

ALT	Active-layer thickness
CRU	Climatic Research Unit
GCM	Global climate models
MAGST	Mean annual ground surface temperature
MAGT	Mean annual ground temperature at the bottom of seasonal freeze-thaw layer
MDGT	Mean decadal ground temperature at the bottom of seasonal freeze-thaw layer
NPS	National Park Service
SNAP	Scenario Network for Arctic and Alaska Planning
SFLT	Seasonally-frozen layer thickness
WRST	Wrangell-St. Elias National Park and Preserve

1. Introduction

Permafrost is defined as "ground (soil or rock and included ice and organic material) that remains at or below 0°C for at least two consecutive years, for natural climatic reasons" (van Everdingen 1998). Permafrost and permafrost-affected regions underlie ~22% of the exposed land in the Northern hemisphere (Brown et al. 1997) and ~80% of Alaska (Jorgenson et al. 2008a). Permafrost terrain consists of an "active layer" at the surface that thaws in summer and freezes again in winter (Muller 1947). The active layer is critical to the ecology and hydrology of permafrost terrain as it provides a rooting zone for plants and acts as a seasonal aquifer for near-surface ground water (Burn 1998). Its thickness is highly variable and can be anywhere from a few decimeters to several meters, depending on the local microclimatic condition, topography, local hydrology, thickness of surface organic layer, vegetation type, and winter snow condition. Similarly, the form and texture of ground ice within permafrost also varies greatly. Ground ice forms include thin lenses of ice, layered ice, reticulated vein ice, and ice wedges as big as 2-4 m long and 3-5 m deep (French and Shur 2010, Kanevskiy et al. 2011).

Permafrost is pervasive in Alaska's National Parks, Preserves, and Monuments. Nearly 40 million acres of Alaska's National Park Service (NPS) units lie within the zone of continuous or discontinuous permafrost. This area constitutes over 70% of Alaska's NPS land and nearly half of all the NPS administered land in the US. Much of this permafrost is vulnerable to major changes due to climatic warming because 1) it has temperatures within a few degrees of freezing, such that relatively minor warming could destabilize it entirely, and/or 2) it contains ice-rich material near the surface that could thaw with climatic warming, leading to major reconfiguration of the landscape through the development of thermokarst (an irregular topography resulting from melting of excess ground ice). Thawing of permafrost could have many consequences, such as drainage of thermokarst lakes, creation of new thaw ponds, soil erosion, thaw slumps, increased sediment loads and siltation of streams and lakes, release of greenhouse gasses, and changes in soil wetness and nutrient cycling. Thawing permafrost is second only to wildfires as a major disturbance to boreal forests (Jorgenson and Osterkamp 2005). Permafrost has been identified by the Arctic and Central Alaska Network as one of the "vital signs" of ecosystem health in Alaska's national parks (MacCluskie and Oakley 2005, Lawler et al. 2009).

Permafrost is a subsurface feature that is difficult to observe and map directly. Temperature measurements are required to determine the status of permafrost and warming permafrost is in danger of thawing (Osterkamp and Jorgenson 2009). Existing information about the distribution and temperature of permafrost in NPS units is limited due to the lack of borehole observations on NPS lands. Modeling of permafrost distribution has proven very useful for extrapolating between widely spaced boreholes where direct observations are made. Permafrost distribution and the thickness of the active layer can be modeled, given sufficient data about soil and ground properties, vegetation, topography, atmospheric climate, and soil temperatures. The same models used to map current permafrost distribution and active-layer thickness can be used to predict the future state of permafrost by using projected climate forcing and scenarios.

Geophysical Institute Permafrost Laboratory (GIPL) at University of Alaska Fairbanks has developed a model, "GIPL 1.0 - Spatially Distributed Model of Permafrost Dynamics in Alaska", that has successfully mapped permafrost distribution and active-layer thickness (ALT) at kilometer scale for the State of Alaska (Marchenko et al. 2008). The GIPL 1.0 model gives a good representation of the coupling between permafrost and the atmosphere. It shows an accuracy of ±0.2 – 0.4°C for the mean annual ground temperature and ±0.1 – 0.3 m for the active-layer thickness calculations when applied to long-term (decadal and longer time scale) averages (Sazonova and Romanovsky 2003). As a part of its inventory and monitoring program, the NPS has obtained or is in the process of gathering data that can be used to make improved runs of the GIPL 1.0 model for NPS units in Alaska.

The goal of this project is to facilitate cooperation between NPS and GIPL to obtain improved and higher-resolution maps for NPS lands of permafrost distribution, temperature, and active-layer thickness under various climate scenarios, including present conditions, the recent past (e.g., 1950, prior to recently observed warming), and the future. The NPS environmental data (soil landscape and ecotype maps) along with past and projected climate forcing and scenarios from global climate datasets are used to create maps of near-surface permafrost distribution and its temperature, and active-layer thickness, for the recent past (1950s), the present (2000s), and the future (2050s and 2090s). Field observation of permafrost presence/absence, summer thaw depth, and ground temperature records from NPS climate stations are used to assess the overall accuracy of the modeled permafrost maps.

2. Wrangell-St. Elias National Park and Preserve (WRST)

The Wrangell-St. Elias National Park and Preserve (WRST) is the largest park unit in the nation. It occupies 13.2 million acres of land in southcentral Alaska (Figure 1). Nearly 10 million acres within the park are designated and managed as wilderness, making this the largest wilderness area within the National Park System. It spans three climate zones (coastal, transitional, and continental), includes four major mountain ranges, and shares 129 miles of coastline along the Gulf of Alaska (http://science.nature.nps.gov/im/units/cakn/WRST.cfm). Due to its vast size and varied climate, the diversity of plant and animal communities in WRST is unsurpassed by any other park unit in Alaska.

Permafrost distribution can be classified as continuous (>90% of land area underlain by permafrost), discontinuous (90% – 50%), sporadic (50% – 10%), or isolated (<10%) (Ferrians 1965). In WRST, permafrost distribution is discontinuous and it contains some of the southern-most warm (fragile) permafrost which is typically within a few degrees of freezing (Drazkowski et al. 2011). Nonetheless, detail information on permafrost condition and distribution within WRST is lacking. The best permafrost information available to date is the limited point observations which are inadequate to determine the condition and distribution of permafrost and consequently the vulnerability of permafrost and WRST landscape to climate change in unknown. Some recent borehole temperature measurements showed significant permafrost warming throughout the Alaska since 1980s (Osterkamp 2007, Romanovsky et al. 2010a, 2010b). Thawing permafrost and thermokarst terrain have also been observed near this park (Jorgenson et al. 2000, Osterkamp et al. 2000). Permafrost is the physical foundation on which the ecosystems in the park rest and thawing of ice-rich permafrost alters this foundation. Permafrost thaw has the potential to greatly alter ecosystems and their net carbon balance i.e., the difference between carbon uptake and emission. In lowlands, a shift from boreal forests to shrubby wetlands or grasslands often occurs with concurrent changes in wildlife populations (Jorgenson et al. 2001). Tracking the distribution and condition of permafrost and development of thermokarst within WRST will provide information about one of the most important drivers of landscape change in the 21st century (http://science.nature.nps.gov/im/units/cakn/VitalSignDetail.cfm?vsid=43).

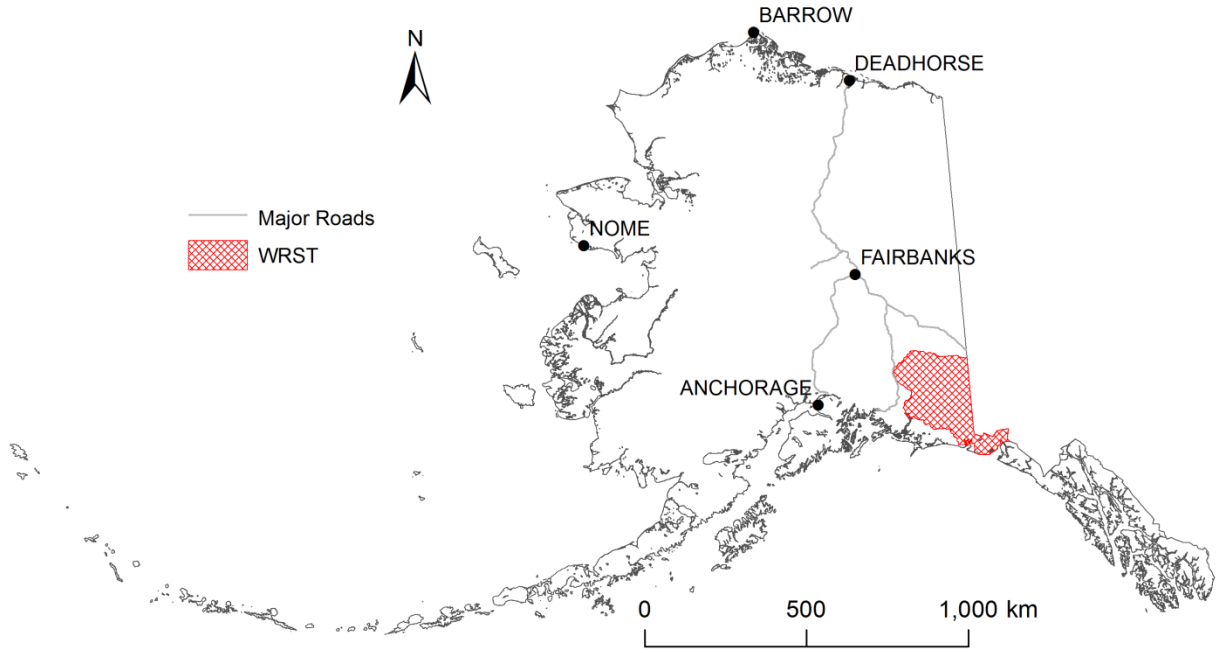

Figure 1. Location of Wrangell St.-Elias National Park and Preserve (WRST) in Alaska.

3. GIPL 1.0 Model

GIPL 1.0 is a quasi-transitional, spatially distributed, equilibrium model for calculating the mean annual temperature at the ground surface and bottom of seasonal freeze-thaw layer, and thickness of seasonal freeze-thaw layer. In the absence of permafrost the seasonal freeze-thaw layer is called "seasonally-frozen layer" (the top layer of the ground that freezes in winter and thaws back in summer and does not have permafrost underneath). The model accounts for the effects of snow cover, surface vegetation, soil moisture, and soil thermal properties (Figure B1). Refer to Appendix B for detailed description of this model.

3.1. GIPL 1.0 Model Input

3.1.1 Climate Data

We used historical (1901 – 2009) monthly average air temperature (°C) and total precipitation (mm) data, CRU TS 3.1 from the University of East Anglia (UK) Climatic Research Unit, downscaled to 771 m by Scenario Network for Alaska & Arctic Planning (SNAP) for past climate forcing (SNAP 2012). Projected (2001 - 2100) monthly average air temperature (°C) and total precipitation (mm) data are available from Fourth Assessment Report (AR4) Global Climate Models (GCM) for a range of possible emission scenarios. Walsh et al. (2008) identified 5 out of a set of 15 global models used in the Coupled Model Intercomparison Project (CMIP) as best performer for Alaska and Greenland. Those 5 AR4 GCMs are:

- cccma_cgcm31: Canadian Centre for Climate Modeling and Analysis, Coupled General Circulation Model version 3.1 – t47, Canada
- mpi_echam5: Max Planck Institute for Meteorology, European Centre Hamburg Model 5, Germany
- gfdl_cm21: Geophysical Fluid Dynamics Laboratory, Coupled Model 2.1, United States
- ukmo_hadcm3: UK Met Office – Hadley Centre, Coupled Model version 3.0, United Kingdom
- miroc3_2_medres: Center for Climate System Research, Model for Interdisciplinary Research on Climate 3.2 (medres), Japan

SNAP averaged the monthly average air temperature and total precipitation projections from the above 5 models for 3 possible emission scenarios (B1: low, A1B: moderate, and A2: high) and created a composite climate dataset for Alaska downscaled to 771 m (SNAP 2012). We used the 5-GCM composite climate dataset for A1B emission scenario as the future climate forcing for the GIPL 1.0 model runs.

3.1.2 Ecotype Data

Sixty-six ecotypes are mapped within WRST (Jorgenson et al. 2008). The ecotypes are mapped by combining climate zone, physiography (e.g., riverine, coastal), topography (DEM), and vegetation

from a landcover spectral database (Stumpf 2007) derived from Landsat ETM+ satellite images. Vegetation was classified to Level IV of the Alaska Vegetation Classification (Viereck et al. 1992).

Surface organic layer thickness and its thermal diffusivity are the two essential ecotype parameters required for ground temperature modeling. Both of these parameters are not available for WRST ecotypes and are thus prescribed. We prescribed surface organic layer thickness based on the vegetation types and their site characteristics in each ecotype and thermal diffusivity values based on our modeling experience in other parts of Alaska. The following ecotype properties are used as the model input (Table A1):

- Thawed thermal diffusivity (m^2/s)
- Frozen thermal diffusivity (m^2/s)
- Surface organic layer thickness (m)

3.1.3 Soil Data

Twenty-one soil landscape classes are identified within WRST (Jorgenson et al. 2008). Soil landscapes are aggregations of similar ecotypes with similar soils, and thus the soil landscape map is in essence the ecotype map described above – populated with soil attributes. They partition the region into landscapes with similar geomorphic processes, soil characteristics, hydrologic regimes, and vegetation with similar composition that are related through successional sequences. We used the soil landscape map as soil map model input. We prescribed the following thermal properties to each soil landscape unit as the model input (Yershov 1984; Table A2):

- Thawed heat capacity (J/m^3K)
- Frozen heat capacity (J/m^3K)
- Thawed thermal conductivity (W/m*K)
- Frozen thermal conductivity (W/m*K)
- Volumetric water content (Fraction of 1)

3.1.4 Snow Data

Snow cover plays an important role in the heat exchange processes between the land surface and the atmosphere. The warming effect of the snow cover has been calculated using approximate formulas derived by Lachenbruch (1959) and Romanovsky (1987), which incorporate ground properties, vegetation cover, and their respective effect on heat turnovers through the snow. Heat turnovers are defined as the quantity of incident heat (during the heating period), or out-going heat (during the cooling period) throughout the medium over a given time interval (usually half year increments). The model takes into account only conductive heat transfer through different mediums.

We created a snow map of Alaska by combining the five seasonal snow classes identified by Sturm et al. (1995) with ecotypes from North America Land Cover Characteristics Data Base Version 2.0

(Loveland et al. 1999). Sturm et al. (1995) defined each snow class by a unique ensemble of the physical properties of the snow (depth, density, thermal conductivity, number of layers, and degree of wetting). Ecotypes in the North America Land Cover Characteristics Data Base Version 2.0 are mapped using multi-temporal AVHRR data and other ancillary data sets. The Alaska snow map has twelve classes (this is an unpublished part of the GIPL model) and nine of those snow classes are present in WRST. The following snow properties are used as the model input (Table A3):

- Density of fresh snow (kg/m^3)
- Maximum density of snow (kg/m^3)

3.2. GIPL 1.0 Output

The GIPL 1.0 permafrost model calculates the following permafrost characteristics:

- Mean annual ground surface temperature (MAGST, °C).
- Mean annual ground temperature (MAGT, °C) at the bottom of seasonal freeze-thaw layer.
- Thickness (m) of seasonal freeze-thaw layer.

4. Preparation of Input Data for Modeling

The preparation of input data for the model runs was done in a GIS environment using the program ArcMap 10 (www.esri.com/software/arcgis/arcgis-for-desktop).

4.1 Glacier-Water Mask

We masked out the glaciers and water bodies within WRST as GIPL 1.0 model calculates temperature on and below the land surface only. We generated the Glacier-Water mask by using the following procedure:

- Generated a WRST outline shape file (WRST-Outline.shp) from the WRST landcover (raster) map (Stumpf 2007). Jorgenson et al. (2008) used this landcover map to create the WRST ecotype and soil landscape maps, so these maps are derived from the same raster. We used the WRST outline shape file to subset rest of the input data layers – air temperature, precipitation, and snow maps.
- Reclassified the glacier and water classes identified in the landcover map as 'nodata'.
- Assigned a single class value '1' to rest of the landcover classes.
- The final Glacier-Water mask raster layer (WRST-Glacier-Water-Mask.tif) has a single class value '1' and the glacier and water classes are identified as 'nodata'.
- The Glacier-Water mask raster layer was used to mask out glaciers and water bodies from rest of the model input data layers.

4.2 Climate Forcing

The monthly average air temperature and monthly total precipitation data, from CRU TS 3.1 and 5-GCM composite, are available at 771m and 800 m cell sizes, respectively, for the entire state of Alaska (SNAP 2012). We used the following procedure to prepare the input climate data for model runs:

- Created decadal average air temperature and precipitation raster layers for every month for the time periods of interest i.e., 1950-1959, 2000-2009, 2001-2010, 2051-2060, and 2091-2100.
- Created WRST subsets of the decadal average air temperature and precipitation data from the previous step by using the 'WRST-Outline.shp' shape file.
- Resampled the WRST decadal average air temperature and precipitation data from the previous step to the resolution of WRST landcover map i.e., 28.5 m.
- Masked out the 'glaciers' and 'water bodies' from the resampled decadal average air temperature and precipitation data by using 'WRST-Glacier-Water-Mask.tif' layer.

- Used CRU climate forcing for the time periods1950-1959 and 2000-2009, and 5-GCM climate forcing for the time periods 2001-2010, 2051-2060, and 2091-2100.

- Converted the raster air temperature and precipitation data layers from the previous step to ASCII format as GIPL 1.0 model requires input data to be in ASCII format.

4.3. Ecotype Map

We masked out the glacier and water bodies pixels from the ecotype map (Jorgenson et al. 2008) by using 'WRST-Glacier-Water-Mask.tif' layer. We fixed the sequence of class values by assigning a continuous sequence of numbers '1-66' to the remaining ecotypes. Converted the resulting raster (.tif) ecotype map to ASCII format.

4.4. Soil Landscape Map

We masked out the glacier and water bodies pixels from the soil landscape map (Jorgenson et al. 2008) by using 'WRST-Glacier-Water-Mask.tif' layer. We fixed the sequence of class values by assigning a continuous sequence of numbers '1-21' to the remaining soil landscape classes. Converted the resulting raster (.tif) soil landscape map to ASCII format.

4.5. Snow Map

The Alaska snow map described in Section 3.1.4 is available at 2 km spatial resolution. We used the following procedure to prepare the input WRST snow map for model runs:

- Created WRST subsets of the Alaska snow map by using the 'WRST-Outline.shp' shape file.

- Resampled the WRST snow map from the previous step to 28.5 m spatial (i.e., the resolution of WRST ecotype map).

- Masked out the 'glaciers' and 'water bodies' from the resampled WRST snow map by using 'WRST-Glacier-Water-Mask.tif' layer.

- Reclassified the WRST snow map to have a continuous sequence of class values '1-9', as 9 out of the 12 snow classes identified in Alaska are present within WRST.

- Converted the raster WRST snow map from the previous step to ASCII format.

5. Results

The modeling effort resulted in high-resolution maps for WRST of near-surface permafrost temperature, and active-layer and seasonally-frozen-layer thickness distribution for the decades 1950-1959, 2000-2009, 2001-2010, 2051-2060, and 2091-2100.

5.1. CRU Climate Forcing (1950-1959 and 2000-2009)

In order to understand the past permafrost distribution and changes to its characteristics between 1950s and 2000s, the modeling results using CRU climate forcing should be compared and analyzed (Table 1). The CRU (1950-1959) decadal mean air temperature within WRST ranged from -25.0°C to 4.7°C and the mean was -3.0°C. The CRU (1950-1959) decadal mean annual precipitation ranged from 261-8641 mm and the mean was 1144 mm. The modeled (1950-1959) permafrost temperature within WRST ranged from -17.2 – 0°C and the mean permafrost temperature was -2.2°C, i.e., the majority of near-surface permafrost within WRST was within 2°C of freezing (Figure 2). The modeled (1950-1959) active-layer thickness ranged from 0.07 – 3.23 m and the mean was 1.26 m (Figure 3). The model mapped 74% of the WRST as underlain by near-surface permafrost during 1950s. The CRU decadal (2000-2009) average air temperature was 0.6°C warmer than the 1950-1959 decade (Table 1). Consequently, the mean decadal (2000-2009) permafrost temperature was 0.3°C warmer than that of 1950-1959. The model mapped 72% of the WRST total area as underlain by near-surface permafrost during 2000s (Figure 4 and 5). The percentage of warm permafrost (i.e., permafrost within a degree of freezing) remains same between 1950s and 2000s – 22% of WRST total area. That is the loss of warm permafrost between 1950s and 2000s was balanced out by the formation of equal extent of new permafrost. This is also apparent from the ALT-thinner-than-1m statistics (Table 1). The percentage of park area with ALT-thinner-than-1m increased by 2% i.e., the model mapped new permafrost formation at 2% of the WRST between 1950s and 2000s. Further analysis of temperature, precipitation, and modeled ground temperature maps showed new permafrost formation in the western part of the WRST mostly at places with little or no increase in air temperature and substantial decrease in precipitation. The decadal average precipitation difference between the 2000-2009 and the 1950-1959 decades varies from -260 to 680 mm. The difference is negative in most part of the WRST and positive only around Malaspina Glacier in the southeast corner of WRST. The snow algorithm in the GIPL 1.0 model uses a simple linear approach to convert the winter precipitation to snow depth by assuming a fixed density of the snow so the model calculates thinner snow depth for lower winter precipitation which in turn results in lower insulation from snow during the winter and hence colder ground temperature. The model calculated up to ~0.5°C colder ground temperature at the bottom of seasonal freeze-thaw layer in the 2000-2009 decade than the 1950-1959 decade due to decrease in precipitation.

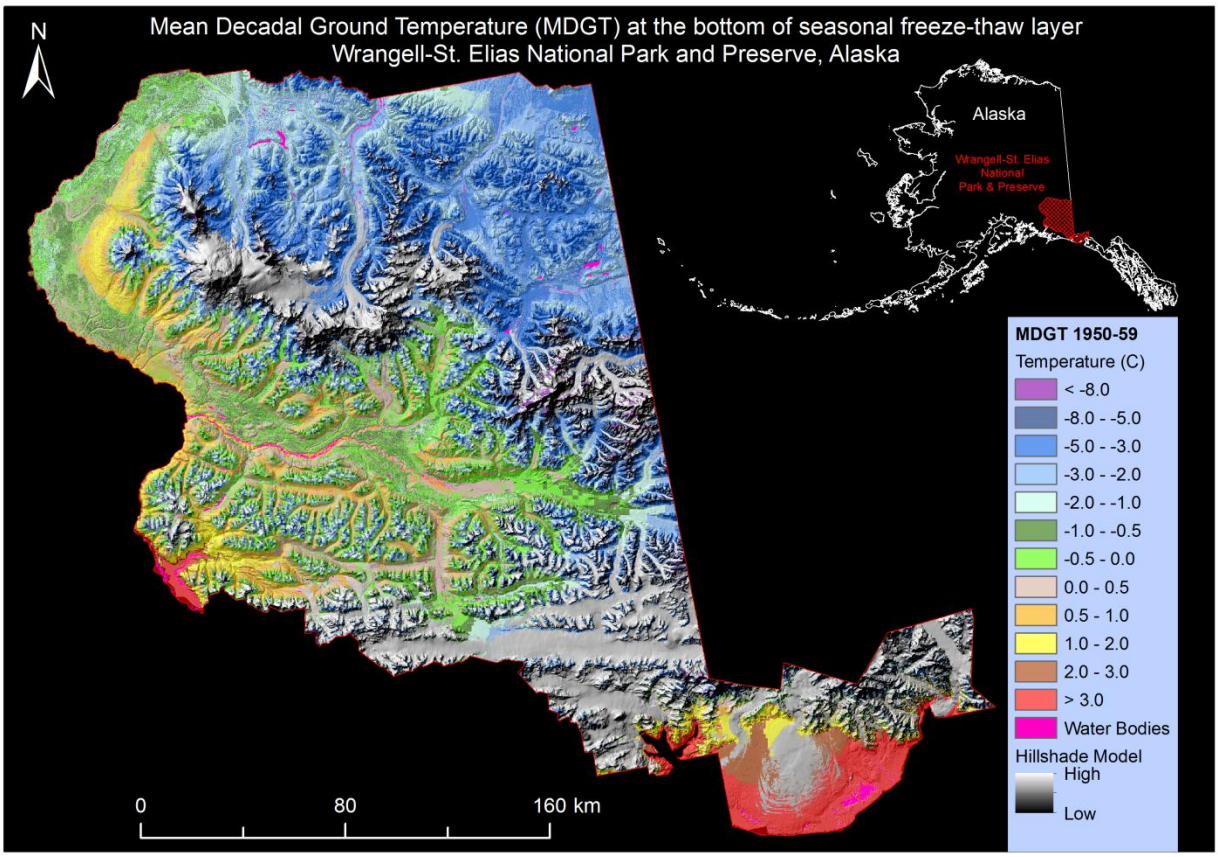

Figure 2. Permafrost map (1950-1959 CRU climate forcing) of Wrangell-St. Elias National Park and Preserve, Alaska. The negative temperature values, shown in shades of green and blue, indicate presence of near-surface permafrost. The positive temperature values, shown in shades of brown and red, indicate absence of near-surface permafrost. The acronym MDGT stands for Mean Decadal Ground Temperature. The MDGT map is draped over a hillshade model shown in grayscale. The hillshade model is apparent in places where glaciers are masked out.

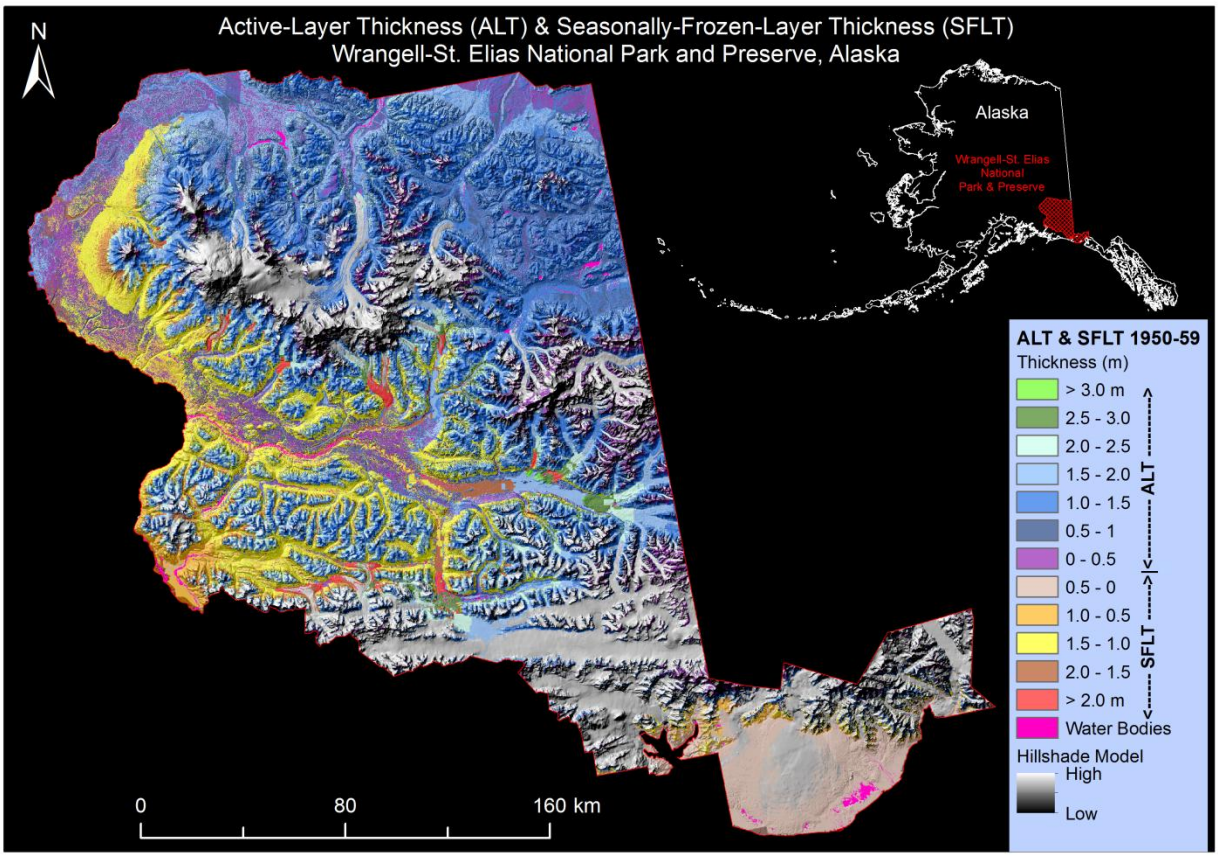

Figure 3. Active-layer and seasonally-frozen-layer thickness map (1950-1959 CRU climate forcing) of Wrangell-St. Elias National Park and Preserve Alaska. The values shown in shades of green, blue, and purple are active-layer thickness (ALT). The values shown in shades of brown and red are seasonally-frozen-layer thickness (SFLT). The ALT and SFLT map is draped over a hill shade model shown in grayscale. The hillshade model is apparent in places where glaciers are masked out.

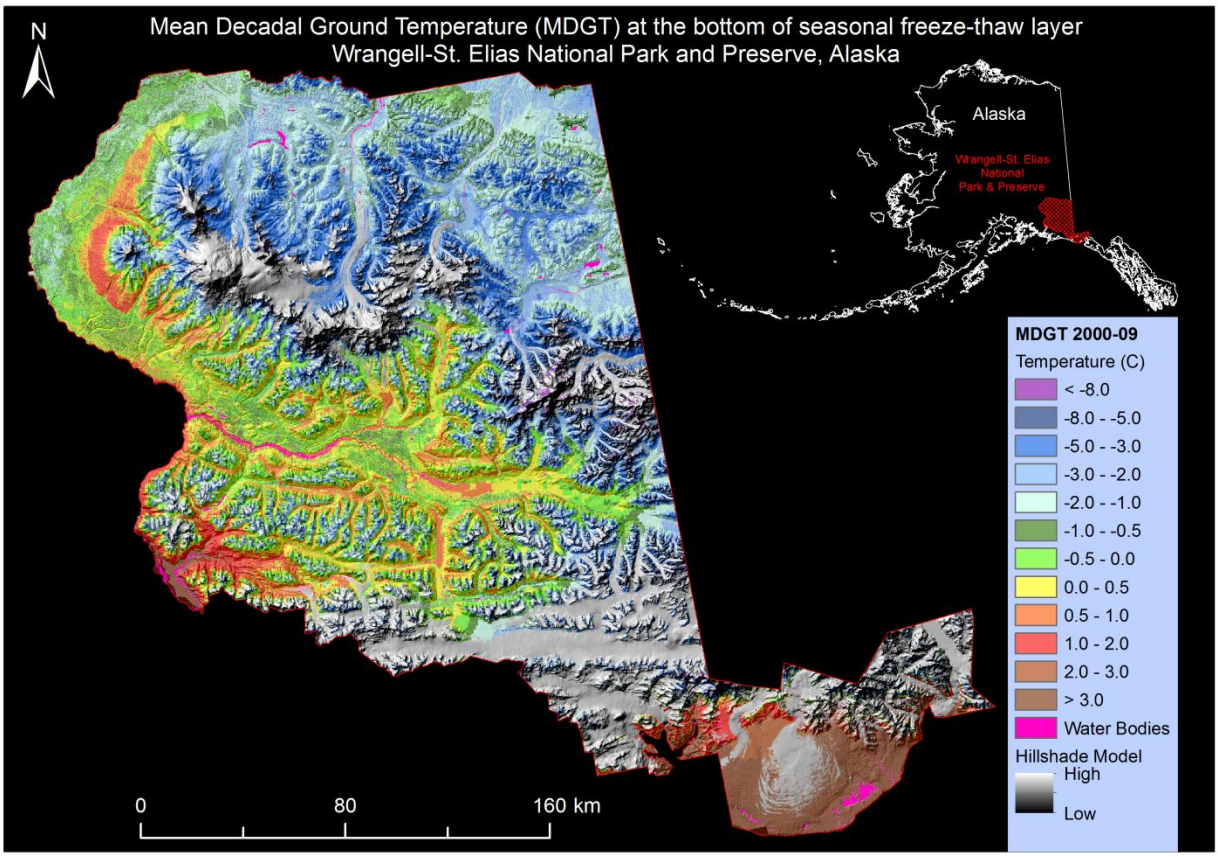

Figure 4. Permafrost map (2000-2009 CRU climate forcing) of Wrangell-St. Elias National Park and Preserve, Alaska. The negative temperature values, shown in shades of green and blue, indicate presence of near-surface permafrost. The positive temperature values, shown in shades of brown and red, indicate absence of near-surface permafrost. The acronym MDGT stands for Mean Decadal Ground Temperature. The MDGT map is draped over a hillshade model shown in grayscale. The hillshade model is apparent in places where glaciers are masked out.

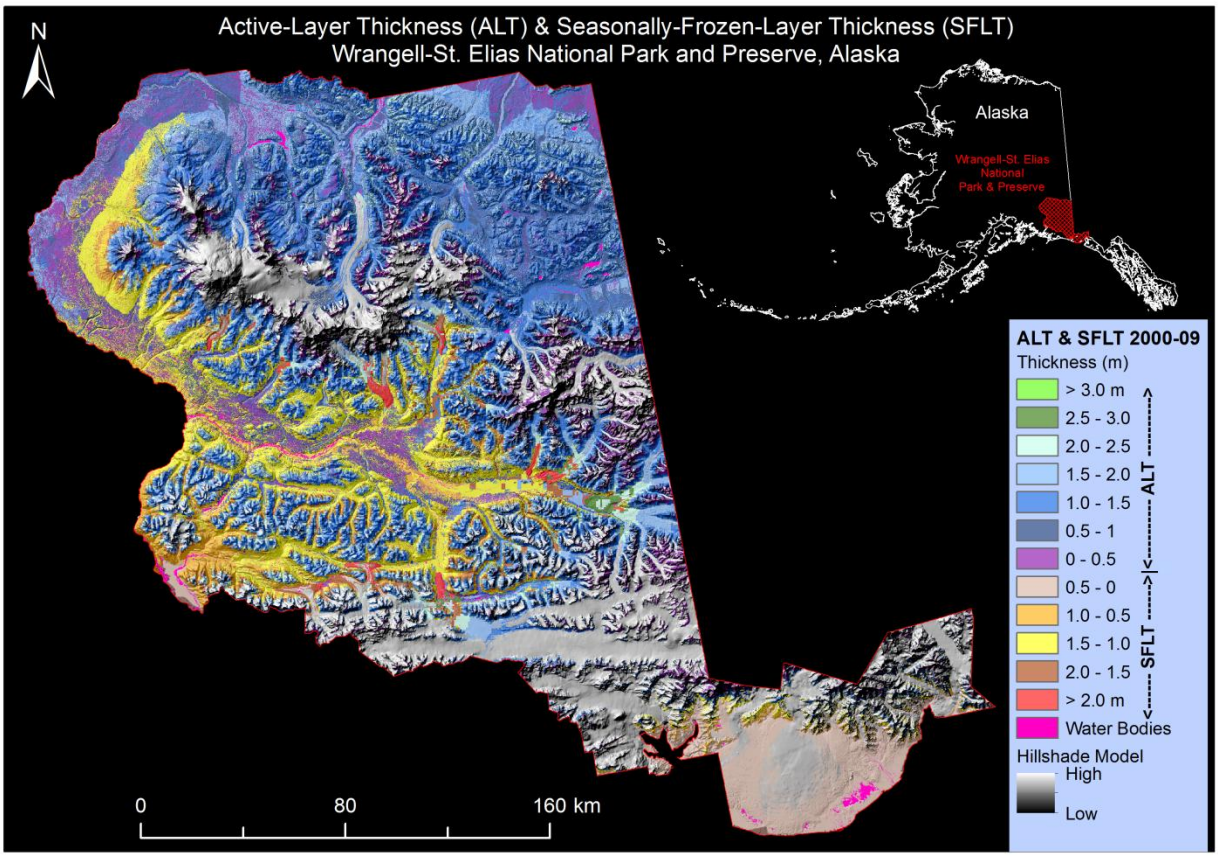

Figure 5. Active-layer and seasonally-frozen-layer thickness map (2000-2009 CRU climate forcing) of Wrangell-St. Elias National Park and Preserve, Alaska. The values shown in shades of green, blue, and purple are active-layer thickness (ALT). The values shown in shades of brown and red are seasonally-frozen-layer thickness (SFLT). The ALT and SFLT map is draped over a hillshade model shown in grayscale. The hillshade model is apparent in places where glaciers are masked out.

Table 1. Summary statistics of climate and modeled permafrost characteristics in Wrangell-St. Elias National Park and Preserve using CRU climate forcing.

Climate characteristics	**1950-1959**	**2000-2009**
Decadal air temperature range (°C)	-25.0 to 4.7	-24.3 to 5.6
Mean decadal air temperature (°C)	-3.0	-2.4
Decadal precipitation range (mm)	261 - 8641	241 – 9031
Mean decadal precipitation (mm)	1144	1110
Modeled permafrost characteristics		
Mean decadal permafrost temperature (°C)	-2.2	-1.9
Permafrost distribution (% of WRST area)	74	72
Permafrost warmer than -1°C (% of WRST area)	22	22
Decadal ALT range (m)	0.07 – 3.23	0.05 – 3.00
Mean decadal ALT (m)	1.26	1.18
Decadal SFLT range (m)	0.05 – 2.75	0 – 2.59
Mean decadal SFLT (m)	1.06	1.0
ALT shallower than 1 m (% of WRST area)	26	28

5.2. 5-GCM Composite Climate Forcing (2001-2010, 2051-2060, and 2091-2100)

The 5-GCM composite decadal (2001-2010) air temperature and precipitation were colder and higher, respectively, than the CRU (2000-2009) air temperature and precipitation. So, the model mapped a greater area of WRST as underlain by near-surface permafrost (80% of WRST total area) during 2001-2010 compared to the model permafrost distribution using CRU (2000-2009) climate forcing. In order to understand the future permafrost distribution and changes to it characteristics due to the projected climate warming the modeling results from 5-GCM composite climate forcing should be compared (Table 2).

The 5-GCM composite decadal (2001-2010) air temperature ranged from - 24.7 to 5.2°C and the mean was -3.0°C. The decadal precipitation ranged from 265 – 10248 mm and the mean was 1288 mm. The model mapped 80% of WRST total area as underlain by near-surface permafrost and the mean permafrost temperature was -2.1°C, i.e., the majority of near-surface permafrost in WRST are within 2°C of freezing (Figure 6 and 7). Also, the model mapped 24% of WRST as underlain by permafrost within a degree of freezing. The 5-GCM composite projected climate data suggests a ~2.0°C warming and 217 mm higher precipitation by 2050s, consequently, the model predicts decrease in near-surface permafrost extent, from 80% of WRST in 2000s to 42% by 2050s (Figure 8 and 9, Table 2). The climate will continue to warm and the climate models suggest another ~2.0°C increase in decadal air temperature by 2090s, i.e., a total of ~4.0°C increase in the air temperature between 2000s and 2090s. This is expected to cause further increase in ground temperature and decrease in near-surface permafrost extent. Only 15% of WRST is predicted to be underlain by 'stable' near-surface permafrost by the end of the 21st century (Figure 10 and 11), i.e., near-surface permafrost in 65% of WRST is predicted to be degrading or completely degraded toward the end of the century. Out of the 15% 'stable' permafrost, more than half would have temperature within a degree of freezing. The model also suggests only 5% of WRST total area will be underlain by

permafrost with ALT-thinner-than-1m by the end of the 21st century compared to 28% of WRST in 2000s.

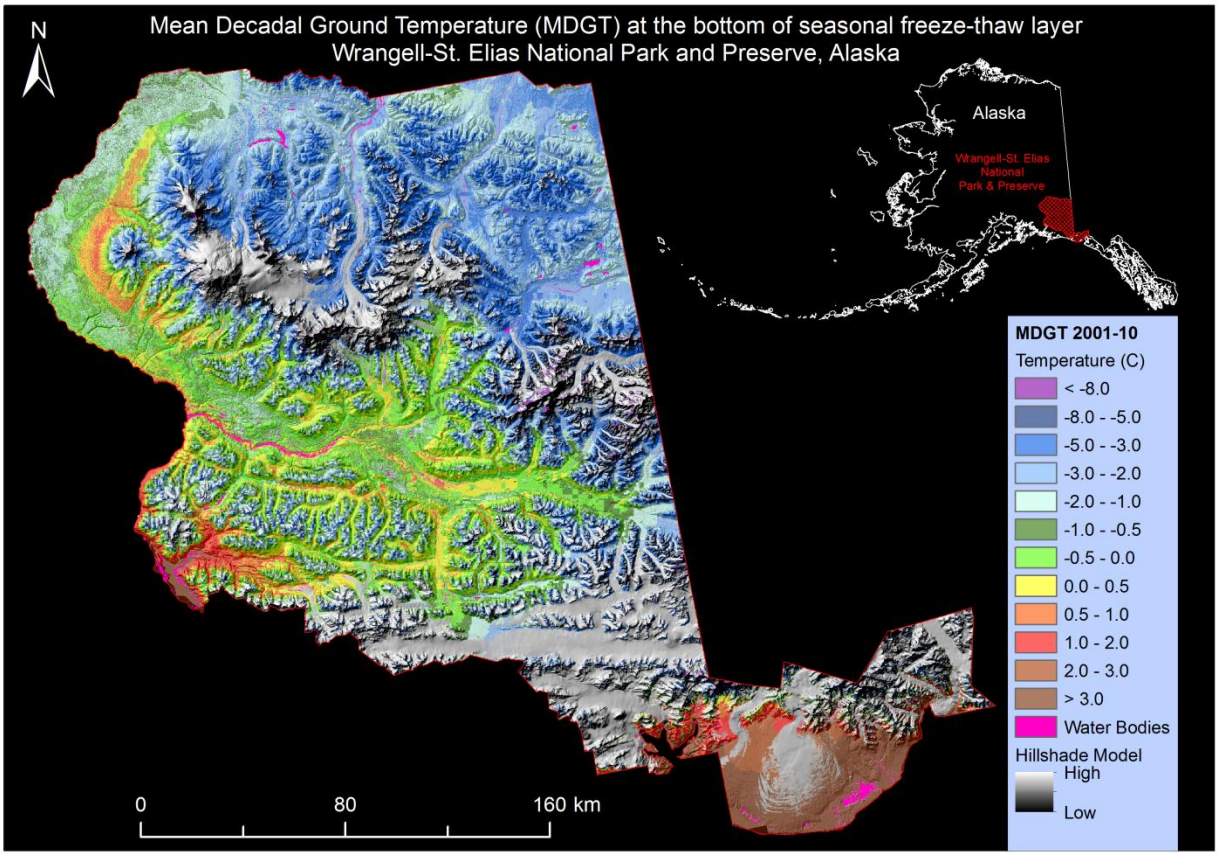

Figure 6. Permafrost map (2001-2010 5-GCM climate forcing) of Wrangell-St. Elias National Park and Preserve, Alaska. The negative temperature values, shown in shades of green and blue, indicate presence of near-surface permafrost. The positive temperature values, shown in shades of brown and red, indicate absence of near-surface permafrost. The acronym MDGT stands for Mean Decadal Ground Temperature. The MDGT map is draped over a hillshade model shown in grayscale. The hillshade model is apparent in places where glaciers are masked out.

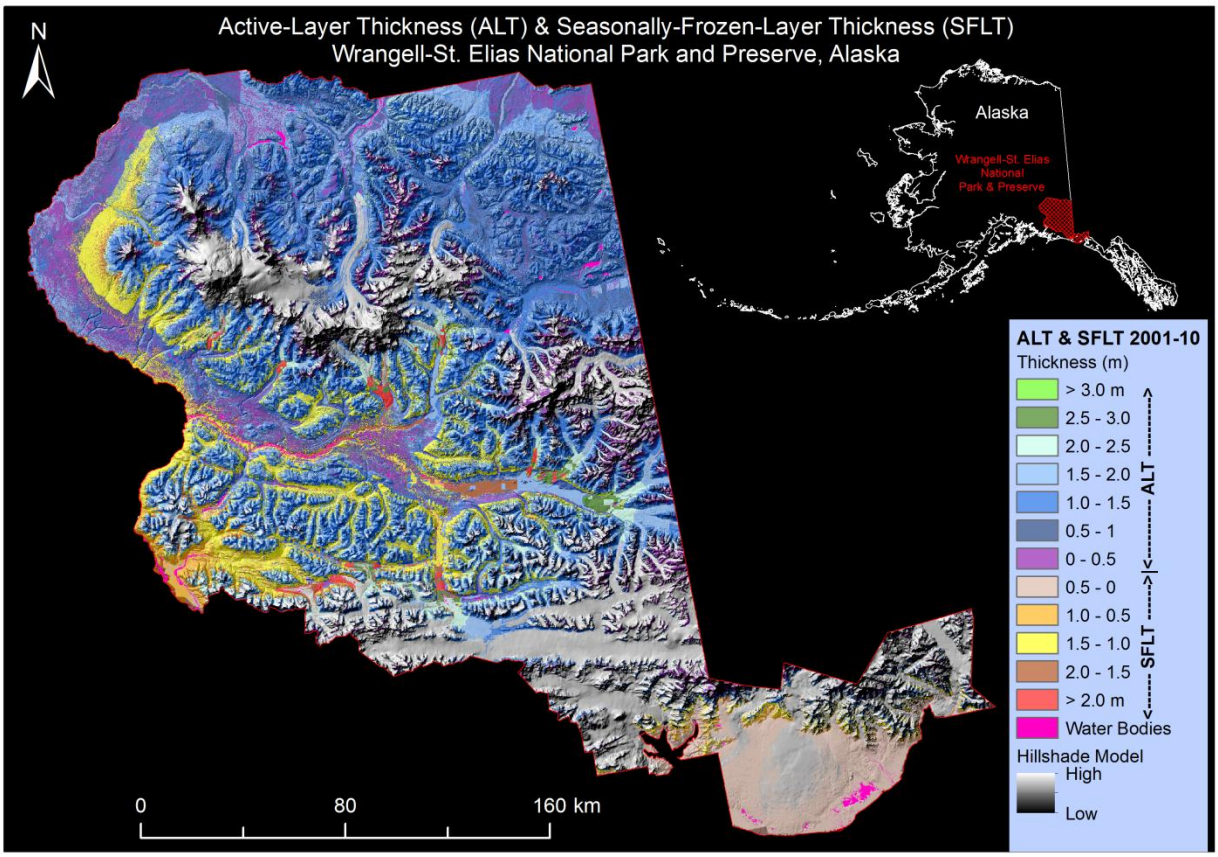

Figure 7. Active-layer and seasonally-frozen-layer thickness map (2001-2010 5-GCM climate forcing) of Wrangell-St. Elias National Park and Preserve, Alaska. The values shown in shades of green, blue, and purple are active- layer thickness (ALT). The values shown in shades of brown and red are seasonally-frozen-layer thickness (SFLT). The ALT and SFLT map is draped over a hillshade model shown in grayscale. The hillshade model is apparent in places where glaciers are masked out.

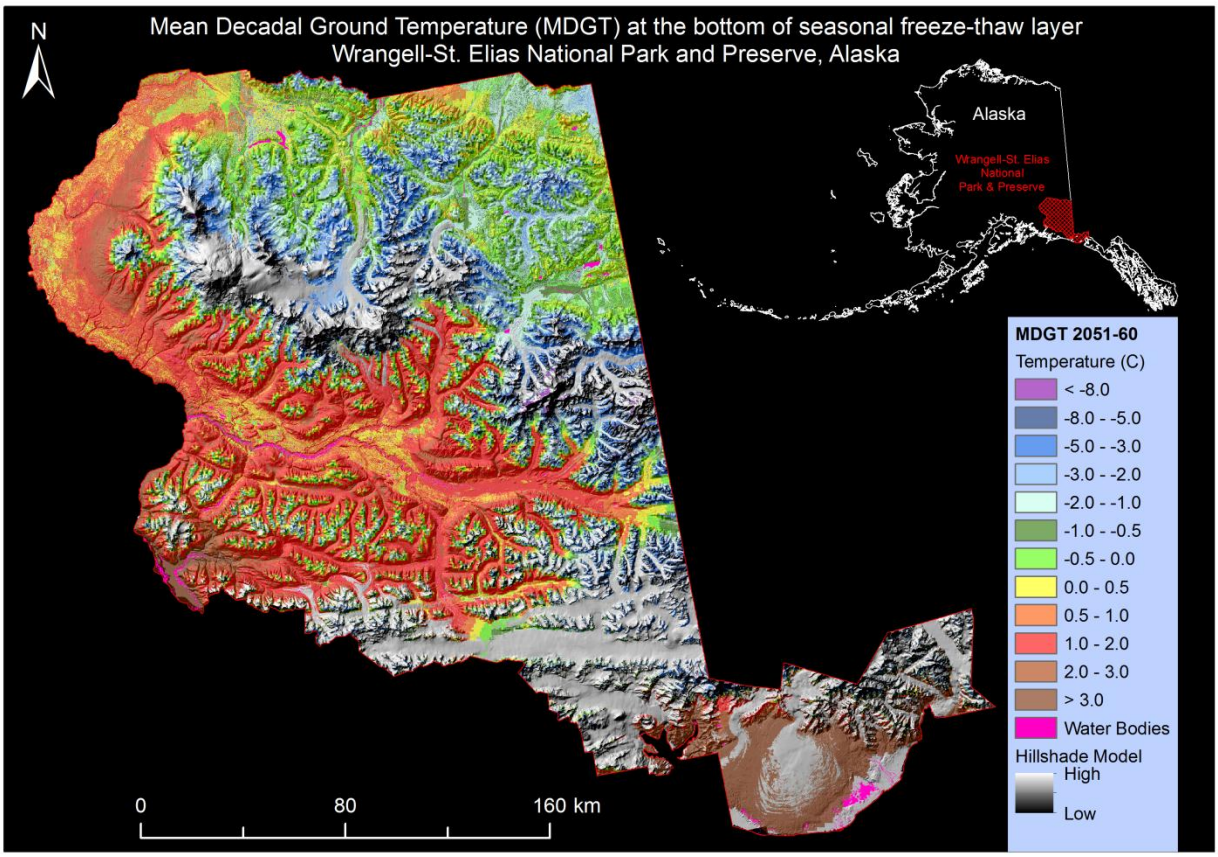

Figure 8. Permafrost map (2051-2060 5-GCM climate forcing) of Wrangell-St. Elias National Park and Preserve, Alaska. The negative temperature values, shown in shades of green and blue, indicate presence of near-surface permafrost. The positive temperature values, shown in shades of brown and red, indicate absence of near-surface permafrost. The acronym MDGT stands for Mean Decadal Ground Temperature. The MDGT map is draped over a hillshade model shown in grayscale. The hillshade model is apparent in places where glaciers are masked out.

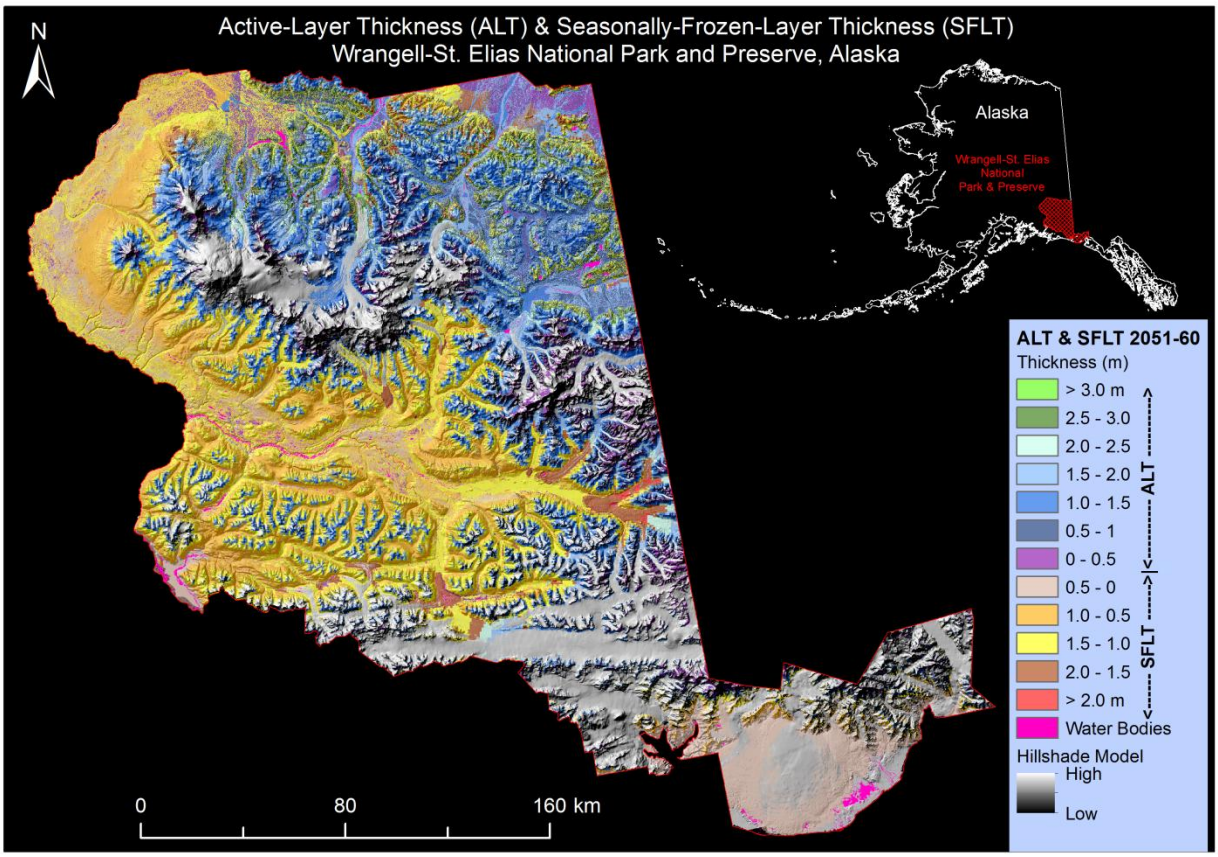

Figure 9. Active-layer and seasonally-frozen-layer thickness map (2051-2060 5-GCM climate forcing) of Wrangell-St. Elias National Park and Preserve, Alaska.The values shown in shades of green, blue, and purple are active- layer thickness (ALT). The values shown in shades of brown and red are seasonally-frozen-layer thickness (SFLT). The ALT and SFLT map is draped over a hillshade model shown in grayscale. The hillshade model is apparent in places where glaciers are masked out.

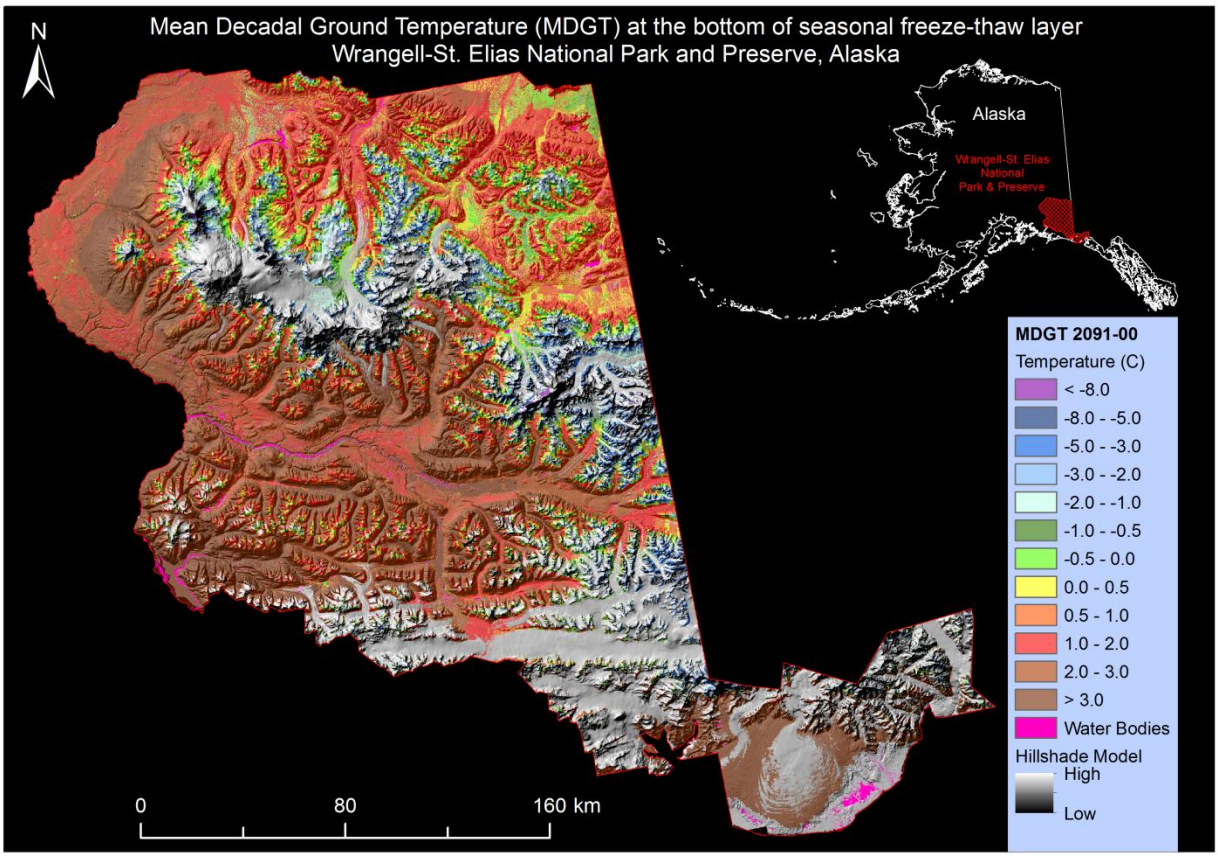

Figure 10. Permafrost map (2091-2100 5-GCM climate forcing) of Wrangell-St. Elias National Park and Preserve, Alaska. The negative temperature values, shown in shades of green and blue, indicate presence of near-surface permafrost. The positive temperature values, shown in shades of brown and red, indicate absence of near-surface permafrost. The acronym MDGT stands for Mean Decadal Ground Temperature. The MDGT map is draped over a hillshade model shown in grayscale. The hillshade model is apparent in places where glaciers are masked out.

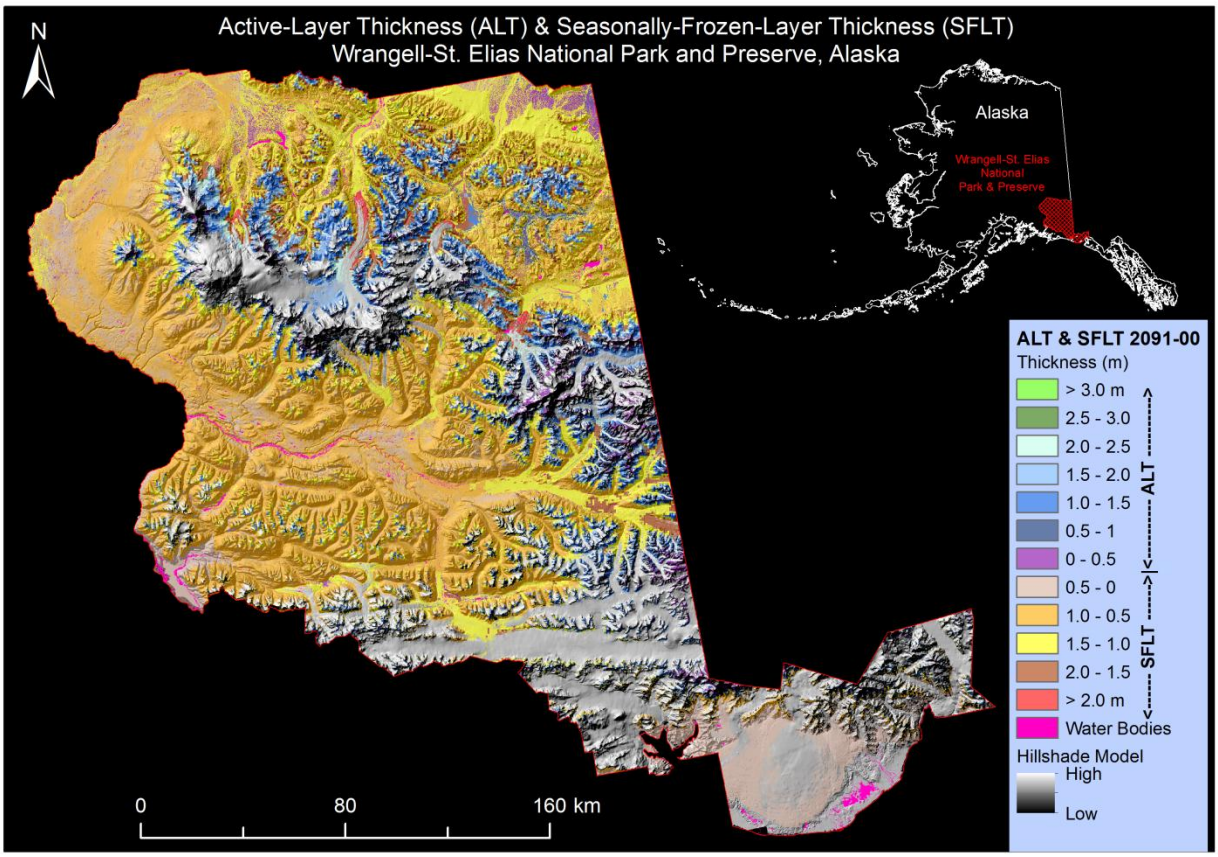

Figure 11. Active-layer and seasonally-frozen-layer thickness map (2091-2100 5-GCM climate forcing) of Wrangell-St. Elias National Park and Preserve, Alaska. The values shown in shades of green, blues, and purple are active layer thickness (ALT). The values shown in shades of brown and red are seasonally-frozen-layer thickness (SFLT). The ALT and SFLT map is draped over a hillshade model shown in grayscale. The hillshade model is apparent in places where glaciers are masked out.

Table 2. Summary statistics of climate and modeled permafrost characteristics in Wrangell-St. Elias National Park and Preserve using 5-GCM composite climate forcing.

Climate characteristics	2001-2010	2051-2060	2091-2100
Decadal air temperature range (°C)	-24.7 – 5.2	-23.0 – 6.9	-21.5 – 8.4
Mean decadal air temperature (°C)	-3.0	-0.9	+0.8
Decadal precipitation range (mm)	265 – 10248	315 –11896	334 – 12378
Mean precipitation (mm)	1288	1505	1591
Modeled permafrost characteristics			
Mean decadal permafrost temperature (°C)	-2.1	-1.5	-1.4
Permafrost distribution (% of WRST area)	80	42	15
Permafrost warmer than -1°C (% of WRST area)	24	18	8
Decadal ALT range (m)	0.06 – 3.11	0.07 – 3.47	0.09 – 3.24
Mean decadal ALT (m)	1.22	1.31	1.32
Decadal SFLT range (m)	0.02 – 2.64	0 – 2.62	0 – 2.5
Mean decadal SFLT (m)	0.93	0.93	0.86
ALT shallower than 1 m (% of WRST area)	28	14	5

5.3. Accuracy Assessment

In order to assess the accuracy of the modeling products we performed two types of tests, warm-biased test and cold-biased test. The warm-biased test tests if the modeled ground temperature is warmer than the actual ground temperature and therefore mapped lesser permafrost extent. The cold-biased test tests if the modeled ground temperature is colder than the actual ground temperature and therefore mapped greater permafrost extent within WRST.

5.3.1. Warm-biased Test

Jorgenson et al. (2008) identified presence/absence of permafrost at 430 field sites sampled during July 2004-2006. They found permafrost at 151 sites out of the 430 sites. We compared the 2000-2009 modeled permafrost map with the field identified permafrost sites. At 8 field-identified permafrost sites, the modeled decadal average ground temperature at the bottom of seasonal freeze-thaw layer are above 0°C i.e., the model predicted absence of near-surface permafrost. However, at the remaining 143 field-identified permafrost sites the modeled permafrost map agrees with field observation. Hence, there is 95% agreement between 2000-2009 modeled permafrost map and field observations that was carried out during 2004-2006. Comparison of the 2001-2010 modeled permafrost map with the field-identified permafrost sites showed agreement at 147 sites, i.e., 97% agreement. This is because the projected 5-GCM composite (2001-2010) air temperatures are colder than the CRU (2000-2009) air temperatures and therefore mapped greater permafrost extent. Since, there are greater than 95% agreement between modeled permafrost presence and field observations of permafrost, the test conclude that the modeling products are not warm-biased.

5.3.2. Cold-biased Test

To test for the cold-bias we compared the permafrost-absent sites identified in the field with modeled permafrost temperature and active-layer thickness at those sites.

Jorgenson et al. (2008) reported permafrost absent at 279 sites. We compared the 2000-2009 modeled permafrost map with the field identified permafrost-absent sites. At 141 sites out of the 279 permafrost-absent sites the model predicted presence of near-surface permafrost and at 100 of these sites Jorgenson et al. (2008) reported maximum depth of investigation. By comparing the model predicted ALT at those 100 sites with the maximum depth of investigation, we found that at 78 sites the modeled ALT is deeper than the maximum depth of investigation which implies the field crew did not investigate deep enough to confirm the presence of permafrost. At the remaining 22 sites the model predicted ALT was shallower than the maximum depth of investigation i.e., at these sites the model falsely predicted presence of permafrost and hence in disagreement with field observations. At 41 sites where maximum depth of investigation was not reported we assumed the field crew must have dug or inserted the frost probe up to 1.0 m depth to confirm the absence of near-surface permafrost. At 11 of these sites the modeled (2000-2009) active-layer thicknesses are shallower than 1.0 m. So, at 33 sites out of the 279 permafrost-absent sites the model falsely predicted presence of permafrost and hence in disagreement with field observations. So the modeled (2000-09) permafrost map is in agreement with field observations at 246 sites or 88% agreement. Comparison of the 2001-2010 modeled permafrost temperature and active-layer thickness at the field-identified permafrost-absent sites showed agreement at 240 sites, i.e., 86% agreement.

The majority of the sites where the model failed are scattered in lowlands along the western and northern border of WRST. The test suggests that the modeling products may be slightly cold-biased at these sites and thus could be mapping greater permafrost extent at those sites.

The warm-biased and cold-biased tests used 151 and 279 field observations within WRST, respectively, to determine the accuracy of the modeling products. The two tests together, in case of both 2000-2009 and 2001-2010 modeled permafrost presence/ absence, resulted in 91% agreement with field observations. Hence, we conclude that the modeled permafrost temperature and active-layer thickness maps are reliable representation of near-surface permafrost and active-layer thickness distribution within WRST. However, we do not rule out the presence of permafrost at a deeper depth where the model did not map near-surface permafrost because GIPL 1.0 is an equilibrium model (Appendix B) and predicts presence or absence of near-surface permafrost only at the bottom of seasonal freeze-thaw layer.

5.3.3. Comparison with Recorded Ground Temperature

NPS has been collecting ground temperature data at few selected depths within the top 1 m of the ground surface at three climate-monitoring stations within WRST since 2005; the stations are Chicken Creek, Chititu, Gates Glacier (http://www.wrcc.dri.edu/wrangell/). We summarized the available ground temperature data from these stations and compared them with the modeled ground temperatures (Table 3).

The average air temperatures at these climate stations are colder than the CRU (by 0.3-1.2°C) and the 5-GCM (by 0.1-0.6°C) decadal air temperatures except at Chicken Creek. We attribute this temperature differences to the difference in scale of the two datasets. The climate station temperature records are from a single location whereas CRU and 5-GCM temperatures are spatially averaged temperature from a global climate datasets of 0.5° x 0.5° latitude-longitude resolution, downscaled to 771 m by SNAP. SNAP utilized PRISM (Parameter-elevation Regressions on Independent Slope Model) spatial climate data at 771 m spatial resolution for downscaling. The PRISM data are developed with a statistical model that accounts for land features such as slope, elevation and coastlines. So the PRISM data assigns a single slope and elevation value to a 771 m cell, but in reality both slope and elevation can vary substantially within a 771 m cell especially in areas of high relief. The three concerned climate stations are located in areas of high relief (Figure 12). Thus the difference in local topography, which strongly influences near-surface air temperature, between the climate stations and 771 m PRISM data cells is majorly responsible for the temperature difference between them. A detail description of the SNAP downscaling procedure can be found here (http://www.snap.uaf.edu/downscaling.php). We further downscaled the CRU and 5-GCM air temperature data by dividing their 771 m cells to 28.5 m cells to be compatible with the soil landscape and ecotype inputs for high-resolution modeling. The difference in the averaging periods, 5-year of climate stations record vs. 10-year of CRU and 5-GCM data, may also be contributing to the temperature difference between them.

The modeled (2000-2009) ground surface temperatures are 0.7°C warmer at Chicken Creek and 2°C colder at Gates Glacier than the recorded ground temperature (at 0.05 m). The modeled (2001-2010) ground surface temperature and recorded ground temperature (at 0.05 m) are same at Chicken Creek and 2.3°C colder at Gates Glacier. This suggests that to some degree the model underestimates the insulating effect of snow as the modeled insulating effect of snow ranges from 1.7 – 2.1°C whereas the recorded temperatures show 1.6°C and 4.4°C difference between near-surface air and ground temperatures (at 0.05 m) at Chicken Creek and Gates Glacier, respectively. This difference can be attributed to three major factors: 1) scale, 2) ground condition, and 3) snow depth. 1) We compared the ground temperature recorded at a single location with modeled (average) ground temperature that used climate inputs derived from global climate datasets of 0.5° x 0.5° latitude-longitude resolution. 2) The difference in ground condition, type and thickness of surface organic layer and seasonal moisture variation, between what really exists at the climate station vs. the generalized ecotype used as the model input. 3) The snow depth at the climate station could be significantly different than the snow depth estimated by the model because the model uses a simple linear approach to convert the winter precipitation to snow depth by assuming a fixed density of the snow which depends on the type of snow at that location. The snow algorithm does not model the effect of wind on snow distribution. Also, both precipitation inputs and snow classes are derived from km scale datasets. So the true snow depth and density at a point location can be significantly different than what used as the model input for that location.

Table 3. Comparison of recorded air and ground temperatures at the NPS climate stations with projected air temperature and modeled temperature at the ground surface and bottom of seasonal freeze-thaw layer. The temperature averaging periods are in parentheses (Note: we summarized ground temperature data only for years that have >=350 days of data).

Recorded	**Chicken Creek Lat: 62.12 °N Lon: 141.84 °W**	**Chititu Lat: 61.27 °N Lon: 142.62 °W**	**Gates Glacier Lat: 61.60 °N Lon: 143.01 °W**
Average air temperature	-3.5°C (2005-2010)	-2.5°C (2005-2008)	-2.0°C (2006-2009)
Average ground temperature at 0.05 m	-1.9°C (2005-2009)	-	2.4°C (2007-2010)
Average ground temperature at 0.5 m	-2.6°C (2005-2009)	-2.3°C (2007-2008, 2010)	2.6°C (2007-2010)
Average ground temperature at 1 m	-2.3°C (2005-2009)	-	2.5°C (2007-2010)
Projected			
CRU average air temperature (2000-2009)	-3.2°C	-1.3°C	-1.3°C
5-GCM average air temperature (2001-2010)	-4.0°C	-1.9°C	-1.9°C
Modeled			
Ground surface temperature (Input: CRU 2000-2009)	-1.2°C	0.5°C	0.4°C
Ground temperature at the bottom of seasonal freeze-thaw layer (Input: CRU 2000-2009)	-1.3°C at 1.26 m	0.1°C at 1.68 m	0.3°C at 1.15 m
Ground surface temperature (Input: 5-GCM 2001-2010)	-1.9°C	0.1°C	0.1°C
Ground temperature at the bottom of seasonal freeze-thaw layer (Input: 5-GCM 2001-2010)	-1.9°C at 1.22 m	-0.3°C at 2.29 m	0.05°C at 1.24 m

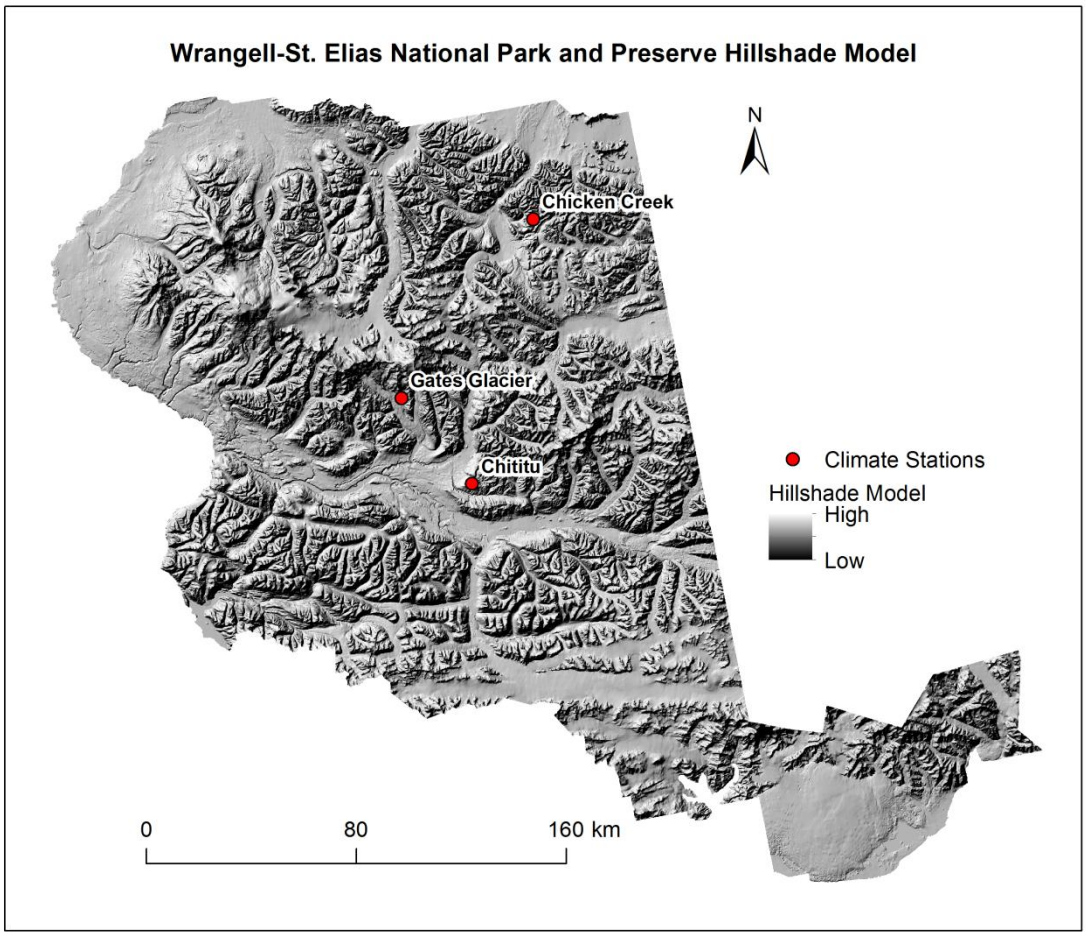

Figure 12. Locations of three climate stations plotted on a Wrangell-St. Elias National Park and Preserve Hillshade Model. The Hillshade Model is derived from 2-arc-second (~60 m) spatial resolution National Elevation Dataset Digital Elevation Model.

6. Deliverables

Deliverables for this project include the following raster (.tif and .png) and legend (.lyr) data files:

- Mean decadal ground temperature, at the bottom of seasonal freeze-thaw layer, raster (WRST-MDGT-####-##.tif) layers of Wrangell-St. Elias National Park and Preserve for the time periods 1950-1959, 2000-2009, 2001-2010, 2051-2060, and 2091-2100.
- Mean decadal ground temperature legend (WRST-MDGT-Legend.lyr) file.
- Mean decadal ground temperature maps (WRST-MDGT-Map-####-##.png) for the time periods 1950-1959, 2000-2009, 2001-2010, 2051-2060, and 2091-2100.
- Active-layer and seasonally-frozen-layer thickness rater layers (WRST-ALT-SFLT-####-##.tif) of Wrangell-St. Elias National Park and Preserve for the time periods 1950-1959, 2000-2009, 2001-2010, 2051-2060, and 2091-2100.
- Active-layer and seasonally-frozen-layer thickness legend (WRST-ALT-SFLT-Legend.lyr) file.
- Active-layer and seasonally-frozen-layer maps (WRST-ALT-SFLT-####-##.png) for the time periods 1950-1959, 2000-2009, 2001-2010, 2051-2060, and 2091-2100.

7. Literature Cited

Brown, J., O. J. Ferrians, Jr., J. A. Heginbottom, and E. S. Melnikov. 1997. Circum-Arctic map of permafrost and ground ice conditions. CP-45. US Geological Survey, Reston, VA.

Burn, C. R. 1998. The active layer: Two contrasting definitions. Permafrost and Periglacial Processes 9:411–416.

Drazkowski, B., K. J. Stark, M. R. Komp, G. Bernatz, D. Brown, C. Richtman, C. Lee, A. Robertson, and K. Slifka. 2011. Wrangell-St. Elias National Park and Preserve, Natural Resource Condition Assessment. Natural Resource Report NPS/NRSS/WRD/NRR—2011/406. National Park Service, Fort Collins, CO.

Ferrians, O. J., Jr. 1965. Permafrost map of Alaska. United States Geological Survey Miscellaneous Investigation, Map I-445, scale 1:2,500,000.

French, H., and Y. Shur. 2010. The principles of cryostratigraphy. Earth-Science Reviews 101:190–206.

Jorgenson, M. T., and T. E. Osterkamp. 2005. Response of boreal ecosystems to varying modes of permafrost degradation. Canadian Journal of Forest Research 35:2100–2111.

Jorgenson, M. T., C. H. Racine, J. C. Walters, and T. E. Osterkamp. 2001. Permafrost degradation and ecological changes associated with a warming climate in central Alaska. Climate Change 48:551–579.

Jorgenson, M. T., J. E. Roth, B. A. Anderson, M. D. Smith, B. E. Lawhead, and S. F. Schlentner. 2000. Ecological land evaluation for the Yukon training area on Fort Wainwright, Alaska: Permafrost, Disturbance, and Habitat use. Report, Corps of Engineers, U.S. Army Cold Regions Research and Engineering Laboratory, Hanover, NH.

Jorgenson, M. T., J. E. Roth, P. F. Loomis, E. R. Pullman, T. C. Cater, M. S. Duffy, W. A. Davis, and M. J. Macander. 2008. An ecological survey for landcover mapping of Wrangell-St. Elias National Park and Preserve. Natural Resource Technical Report NPS/WRST/NRTR—2008/094. National Park Service, Natural Resource Program Center, Fort Collins, CO.

Jorgenson, M. T., K. Yoshikawa, M. Kanevskiy, and Y. Shur. 2008a. Permafrost characteristics of Alaska. Institute of Northern Engineering, University of Alaska Fairbanks, 1 Sheet, Scale 1: 7,200,000.

Kanevskiy. M., Y. Shur, D. Fortier, M. T. Jorgenson, and E. Stephani. 2011. Cryostratigraphy of late Pleistocene syngenetic permafrost (yedoma) in northern Alaska, Itkillik River exposure. Quaternary Research 75(3):584–596.

Lachenbruch, A. H. 1959. Periodic heat flow in a stratified medium with application to permafrost problems. US Geological Survey Bulletin, 1083-A, 36 p.

Lawler, J. P., S. D. Miller, D. M. Sanzone, J. Ver Hoef, and S. B. Young. 2009. Arctic network vital signs monitoring plan. Natural Resource Report NPS/ARCN/NRR—2009/088. U.S. Department of the Interior, National Park Service, Natural Resource Program Center, Ft. Collins, CO.

Loveland, T. R., Z. Zhu, D. O. Ohlen, J. F. Brown, B. C. Reed, L. Yang. 1999. An analysis of the IGBP global land-cover characterization process. Photogrammetric Engineering and Remote Sensing 65(9):1021–32.

MacCluskie, M., and K. Oakley. 2005. Vital signs monitoring plan, Central Alaska Network. August 2005. U.S. Department of the Interior, National Park Service, Fairbanks, AK.

Marchenko, S., V. Romanovsky, and G. Tipenko. 2008. Numerical modeling of spatial permafrost dynamics in Alaska. In the Proceedings of Ninth International Conference on Permafrost, June 2008, Vol. 2: 1125–30.

Muller, S. W. 1947. Permafrost or permanently frozen ground and related engineering problems. W. Edwards, Inc., Ann Arbor, MI. 231 p.

Osterkamp, T. E. 2007. Characteristics of the recent warming of permafrost in Alaska. Journal of Geophysical Research 112:F02S02, doi:10.1029/2006JF000578.

Osterkamp, T. E., and M. T. Jorgenson. 2009. Permafrost conditions and processes. Pages 205–227 *in* R. Young and L. Norby, editors. Geological monitoring: Boulder, Colorado, Geological Society of America.

Osterkamp, T. E., L. Viereck, Y. Shur, M. T. Jorgenson, C. Racine, A. Doyle, and R. D. Boone. 2000. Observation of thermokarst and its impact on boreal forests in Alaska, U.S.A. Arctic, Antarctic, and Alpine Research 32(3):303–315

Romanovsky, V. E. 1987. Approximate calculation of the insulation effect of the snow cover. Geokriologicheskie Issledovania (in Russian), MGU Press 23:145–157.

Romanovsky, V. E., Y. Shur, K. Yoshikawa, and G. S. Tipenko. 2010a. Establishing a permafrost observatory at the Gakona HAARP site. Permafrost Laboratory. Available at http://permafrost.gi.alaska.edu/project/establishing-permafrost-observatory-gakona-haarp-site (accessed 17 May 2013).

Romanovsky. V. E., S. L. Smith, and H. H. Christiansen. 2010b. Permafrost thermal state in the Polar Northern Hemisphere during the International Polar Year 2007–2009: a synthesis. Permafrost and Periglacial Processes 21:106–116.

Sazonova, T. S., and V. E. Romanovsky. 2003. A model for regional-scale estimation of temporal and spatial variability of active-layer thickness and mean annual ground temperatures. Permafrost and Periglacial Processes 14:125–139.

SNAP (Scenarios Network for Alaska and Arctic Planning). 2012. Tools and Data, Data. Available at http://www.snap.uaf.edu/data.php (accessed 27 January 2012).

Stumpf, K. 2007. Wrangell-St. Elias National Park and Preserve landcover mapping project. Natural Resource Technical Report NPS/WRST/NRTR—2008/095. National Park Service, Fort Collins, CO.

Sturm, M., J. Holmgren, and G. E. Liston. 1995. A seasonal snow cover classification system for local to global applications. Journal of Climate 8(5):1261–1283.

Van Everdingen, R. O. 1998. Multi-language glossary of permafrost and related ground ice terms. International Permafrost Association, National Snow and Ice Data Center, University of Colorado, Boulder.

Viereck, L. A., C. T. Dyrness, A. R. Batten, and K. J. Wenzlick. 1992. The Alaska vegetation classification. General Technical Report, PNW-GTR-286. Pacific Northwest Research Station, U.S. Forest Service, Portland, OR.

Walsh, J. E., W. L. Chapma, V. Romanovsky, J. H. Christensen, and M. Stendel. 2008. Global climate model performance over Alaska and Greenland. America Meteorological Society 21:6156–6174.

Yershov, E. D. 1984. Thermal-physical properties of earth materials. Moscow State University Publication, p. 203 (In Russian).

Appendix A. Tables of Ecotype, Soil Landscape, and Snow Classes

Table A1. Sixty six ecotypes mapped within Wrangell-St. Elias National Park and Preserve by Jorgenson et al. (2008) are used as ecotype input to the model. Eight out of the 66 ecotypes have little or no vegetation on surface (vegetation cover <= 15%) with no surface organic (surface organic depth = 0). We used the surface organic depth reported by Jorgenson et al. (2008) for each ecotype as the organic layer thickness model input.

Ecotype no.	Ecotype name	Thawed diffusivity (m^2/s)	Frozen diffusivity (m^2/s)	Thickness (m)
1	Boreal alpine barrens	$2.48e^{-6}$	$1.29e^{-6}$	0.01
2	Boreal alpine dryas dwarf shrub	$1.0e^{-6}$	$1.0e^{-6}$	0.03
3	Boreal alpine ericaceous dwarf shrub	$1.0e^{-6}$	$1.0e^{-6}$	0.04
4	Boreal alpine sedge-dwarf willow meadow	$1.1e^{-6}$	$1.1e^{-6}$	0.07
5	Boreal alpine sedge meadow	$1.26e^{-7}$	$1.43e^{-6}$	0.3
6	Boreal alpine tussock meadow	$1.18e^{-7}$	$1.12e^{-6}$	0.15
7	Boreal glaciated barrens	-	-	0.0
8	Boreal glaciated dryas dwarf shrub	$1.1e^{-6}$	$1.1e^{-6}$	0.02
9	Boreal glaciated poplar forests	$5.06e^{-5}$	$3.06e^{-5}$	0.01
10	Boreal glaciated willow shrub	$1.0e^{-6}$	$1.0e^{-6}$	0.02
11	Boreal lacustrine sedge meadow	$1.9e^{-6}$	$1.0e^{-6}$	0.5
12	Boreal lowland barrens	-	-	0.0
13	Boreal lowland black spruce bog	$1.01e^{-6}$	$2.01e^{-6}$	0.3
14	Boreal lowland black spruce forest	$1.47e^{-6}$	$3.74e^{-6}$	0.13
15	Boreal lowland low birch-willow shrub	$2.01e^{-6}$	$1.01e^{-6}$	0.1
16	Boreal lowland sedge-shrub fen	$1.97e^{-6}$	$1.02e^{-6}$	0.7
17	Boreal lowland tall willow shrub	$1.97e^{-6}$	$1.02e^{-6}$	0.02
18	Boreal lowland tussock-shrub bog	$1.05e^{-6}$	$1.95e^{-6}$	0.3
19	Boreal lowland white spruce forest	$1.48e^{-6}$	$1.84e^{-6}$	0.2
20	Boreal riverine circumalkaline barrens	-	-	0.0
21	Boreal riverine dryas dwarf shrub	$1.08e^{-6}$	$1.13e^{-6}$	0.01
22	Boreal riverine gravelly poplar forest	$2.06e^{-6}$	$1.06e^{-6}$	0.01
23	Boreal riverine loamy poplar forest	$5.06e^{-6}$	$5.06e^{-6}$	0.02
24	Boreal riverine loamy willow shrub	$1.57e^{-6}$	$1.02e^{-6}$	0.04
25	Boreal riverine low silverberry shrub	$1.37e^{-6}$	$1.02e^{-6}$	0.01
26	Boreal riverine sandy willow shrub	$1.47e^{-6}$	$1.02e^{-6}$	0.02
27	Boreal riverine spruce-poplar forest	$1.36e^{-6}$	$1.06e^{-6}$	0.04
28	Boreal riverine tall alder shrub	$1.37e^{-6}$	$1.02e^{-6}$	0.01
29	Boreal riverine white spruce forest	$1.36e^{-6}$	$1.06e^{-6}$	0.04
30	Boreal subalpine forb meadow	$1.48e^{-6}$	$1.13e^{-6}$	0.09
31	Boreal subalpine poplar forest	$2.16e^{-6}$	$2.06e^{-6}$	0.09
32	Boreal subalpine spruce woodland	$1.08e^{-6}$	$1.89e^{-6}$	0.06
33	Boreal subalpine willow and birch shrub	$1.47e^{-6}$	$1.02e^{-6}$	0.07

Ecotype no.	Ecotype name	Thawed diffusivity (m^2/s)	Frozen diffusivity (m^2/s)	Thickness (m)
34	Boreal upland aspen forest	$1.68e^{-6}$	$1.12e^{-6}$	0.03
35	Boreal upland birch forest	$1.88e^{-6}$	$1.12e^{-6}$	0.1
36	Boreal upland forb meadow	$1.58e^{-6}$	$1.16e^{-6}$	0.09
37	Boreal upland sagebrush meadow	$1.48e^{-6}$	$1.15e^{-6}$	0.01
38	Boreal upland spruce-birch forest	$1.38e^{-6}$	$1.26e^{-6}$	0.13
39	Boreal upland tall alder shrub	$1.87e^{-6}$	$1.22e^{-6}$	0.13
40	Boreal upland tall willow shrub	$1.37e^{-6}$	$1.05e^{-6}$	0.1
41	Boreal upland white spruce forest	$1.58e^{-6}$	$1.17e^{-6}$	0.07
42	Maritime alpine barrens	-	-	0.0
43	Maritime alpine cassiope dwarf shrub	$1.48e^{-6}$	$1.29e^{-6}$	0.02
44	Maritime coastal angelica meadow	$1.58e^{-6}$	$1.13e^{-6}$	0.02
45	Maritime coastal barrens	-	-	0.0
46	Maritime coastal brakish barrens	-	-	0.0
47	Maritime coastal elymus meadow	$1.98e^{-6}$	$1.13e^{-6}$	0.03
48	Maritime glaciated barrens	-	-	0.0
49	Maritime glaciated tall alder-willow shrub	$1.27e^{-6}$	$1.32e^{-6}$	0.02
50	Maritime lowland cottonwood-spruce forest	$1.48e^{-6}$	$1.74e^{-6}$	0.1
51	Maritime lowland cottonwood forest	$1.48e^{-6}$	$1.34e^{-6}$	0.07
52	Maritime lowland forb-willow meadow	$1.68e^{-6}$	$1.17e^{-6}$	0.11
53	Maritime lowland menyanthes bog	$1.55e^{-6}$	$1.84e^{-6}$	0.2
54	Maritime lowland sedge-blueberry bog	$1.35e^{-6}$	$1.45e^{-6}$	0.48
55	Maritime lowland sitka spruce forest	$1.48e^{-6}$	$1.25e^{-6}$	0.07
56	Maritime lowland tall alder-willow shrub	$1.37e^{-6}$	$1.02e^{-6}$	0.15
57	Maritime riverine barrens	-	-	0.0
58	Maritime riverine cottonwood-spruce forest	$1.26e^{-6}$	$1.06e^{-6}$	0.04
59	Maritime riverine cottonwood forest	$1.66e^{-6}$	$1.06e^{-6}$	0.03
60	Maritime riverine horsetail	$1.48e^{-6}$	$1.13e^{-6}$	0.01
61	Maritime riverine tall alder-willow shrub	$1.52e^{-6}$	$1.08e^{-6}$	0.02
62	Maritime riverine tall willow shrub	$1.87e^{-6}$	$1.02e^{-6}$	0.02
63	Maritime subalpine low blueberry shrub	$1.98e^{-6}$	$1.13e^{-6}$	0.03
64	Maritime subalpine lupine meadow	$1.98e^{-6}$	$1.13e^{-6}$	0.02
65	Maritime upland sitka spruce forest	$7.07e^{-7}$	$7.06e^{-7}$	0.16
66	Maritime upland tall alder shrub	$1.87e^{-6}$	$1.02e^{-6}$	0.1

Table A2. Twenty-one soil landscape classes identified within Wrangell-St. Elias National Park and Preserve by Jorgenson et al. (2008) are used as soil type input to the model. The water landscape is excluded from modeling. We referred to Yershov (1984) to prescribe the soil thermal properties.

No.	Soil landscape name	Thawed heat capacity ($MJ/m^3.K$)	Frozen heat capacity ($MJ/m^3.K$)	Thawed thermal conductivity (W/m.K)	Frozen thermal conductivity (W/m.K)	Volumetric water content (%)
1	Boreal alpine organic-rich meadows	2.11	1.97	0.43	1.23	0.5
2	Boreal alpine rocky-loamy meadows	2.2	2.0	1.23	1.56	0.2
3	Boreal alpine rocky barrens and scrub	2.11	1.87	1.65	1.88	0.05
4	Boreal glaciated forests (Boreal glaciated poplar forest)	2.02	1.96	1.36	1.57	0.1
5	Boreal glaciated rocky barrens and scrub	2.34	2.16	1.88	2.1	0.05
6	Boreal lowland loamy scrub and forests	2.02	1.83	1.23	1.63	0.2
7	Boreal lowland organic-rich meadows	2.22	1.8	0.42	1.23	0.5
8	Boreal lowland scrub and forest bogs	2.22	1.8	1.12	1.74	0.5
9	Boreal riverine rocky-loamy barrens and scrub	2.02	2.0	1.76	2.05	0.1
10	Boreal riverine rocky-loamy forests	2.02	1.83	1.15	1.57	0.15
11	Boreal subalpine rocky scrub and woodlands	2.01	1.95	1.89	2.01	0.1
12	Boreal upland rocky-loamy scrub and forests	2.02	1.98	1.43	1.72	0.1
13	Maritime alkaline rocky barrens and scrub	2.11	1.97	1.85	2.02	0.05
14	Maritime coastal barrens and meadows	2.15	1.78	1.46	1.8	0.1
15	Maritime glaciated rocky barrens and scrub	2.21	2.02	1.82	2.21	0.3
16	Maritime lowland bogs and fens	2.15	1.78	1.42	1.95	0.5
17	Maritime lowland gravelly scrub and forests	2.02	1.96	1.96	2.10	0.15
18	Maritime riverine gravelly barrens and scrub	2.02	1.99	1.72	1.89	0.2
19	Maritime riverine gravelly forests	2.02	1.82	1.58	1.82	0.1
20	Maritime subalpine rocky meadows and scrub	2.01	1.95	1.89	2.07	0.1
21	Maritime upland rocky-sandy scrub and forests	2.01	1.95	1.89	2.11	0.1

Table A3. Nine snow classes identified within the Wrangell-St. Elias National Park and Preserve are used as snow input to the model. The snow classes are identified by integrating the snow class from Sturm et al. (1995) with ecotypes from North America Land Cover Characteristics Data Base Version 2.0 (Loveland et al. 1999).

Class no.	Class name	Density of fresh snow (kg/m^3)	Maximum density of snow (kg/m^3)
1	Bare desert	82	320
2	Upland tundra	65	180
3	Alpine	100	320
4	Maritime I	65	185
5	Maritime II	60	140
6	Shrub deciduous	70	220
7	Grassland	100	280
8	Conifer forest	70	220
9	Mixed forest	90	180

Appendix B. The GIPL Model for Estimation of Temporal and Spatial Variability of the Active-Layer Thickness and Mean Annual Ground Temperatures

Sergey S. Marchenko and Vladimir E. Romanovsky

The Geophysical Institute Permafrost Lab (GIPL) model was developed specifically to assess the effect of a changing climate on permafrost. The GIPL 1.0 model is a quasi-transitional, spatially distributed, equilibrium model for calculating the active-layer thickness and mean annual ground temperature. It accounts effectively for the effects of snow cover, vegetation, soil moisture, and soil thermal properties. It allows for the calculation of maximum active-layer thickness (ALT) and mean annual ground temperatures (MAGT) at the bottom of the active layer. Our approach to determine the ALT and MAGT is based on an approximate analytical solution that includes freezing/thawing processes and provides an estimation of thermal offset due to the difference in frozen and thawed soil thermal properties (Kudryavtsev et al. 1974). It uses the idea of applying the Fourier temperature wave propagation theory to a medium with phase transitions, such as freezing/thawing ground. Application of this approach resulted in the discovery of the thermal offset and an understanding of the laws that govern the dynamics of the ground thermal regime. These discoveries led to an understanding of the effects that the thermal properties of the ground have upon the MAGT and ALT, and how periodically (seasonally) varying climatic parameters affect permafrost dynamics. The output parameters of this method are given as annual averages. Input and output parameters are listed in Table B1. The effect of geothermal heat flux is ignored because it is considered to have a minimal impact on the MAGT and ALT values. For the areas with permafrost, the MAGT is the same as a mean annual temperature at the permafrost table (upper surface of permafrost). Where permafrost is absent, the MAGT is the mean annual temperature at the bottom of seasonally-frozen layer.

Table B1. Model input and output variables.

Input Variables	**Notation**	**Units**
Seasonal range of air temperature variations (amplitude)	A_a	ºC
Mean annual air temperature	T_a	ºC
Snow Water Equivalent	SWE	m
Height of vegetation cover	H_v	m
Thermal diffusivity of vegetation in frozen state	D_{vf}	m^2/s
Thermal diffusivity of vegetation in thawed state	D_{vt}	m^2/s
Thermal conductivity of frozen soil	K_f	W/(m*K)
Thermal conductivity of thawed soil	K_{th}	W/(m*K)
Volumetric water content	VWC	Fraction of 1
Volumetric latent heat of ice fusion	334e6	J/m^3
Volumetric heat capacity of snow cover	C_{sn}	J/m^3K
Volumetric heat capacity of thawed ground	C_{th}	J/m^3K
Volumetric heat capacity of frozen ground	C_f	J/m^3K

Input Variables	Notation	Units
Output Variables		**Notation**
Correction to air temperature accounting for snow cover effect, ºC		ΔT_{sn}
Correction to air temperature amplitude accounting for snow cover effect, ºC		ΔA_{sn}
Correction to air temperature accounting for vegetation cover , ºC		ΔT_{v}
Correction to air temperature amplitude accounting for vegetation cover , ºC		ΔA_{v}
Seasonal range of temperature variations at the ground surface, ºC		A_{gs}
Mean annual temperatures at the ground surface, ºC		T_{gs}
Snow density, kg/m^3		ρ_{sn}
Snow thermal conductivity, W/(m*K)		K_{sn}
Thermal offset, ºC		ΔT_{k}
Mean annual soil surface temperature, ºC		MAGST
Mean annual soil temperature at the bottom of ALT , ºC		MAGT
Active-layer thickness, m		ALT

Mean Annual Ground Temperature at the Bottom of the Active Layer

Throughout the years, simplified analytical solutions for the ALT have been applied for structural engineering and other practical purposes. Most of these methods have been based on the Stefan solutions, and they do not yield a good level of accuracy (Romanovsky and Osterkamp 1997). It was determined that the best method for computation of the ALT and MAGT was a modified version of Kudryavtsev's approach (Romanovsky and Osterkamp 1997). This approach is the core of the GIPL 1.0 model, which treats the complex system including air, snow cover, surface vegetation, and active layer, as a set of individual layers with different thermal properties (Figure B1). In the regions of Alaska and East-Siberia that were analyzed, surface vegetation consists of lichens, grass, and moss (sphagnum or feather mosses) (Feldman et al. 1988, Brown and Kreig 1983). The upper level of vegetation consisting of trees and shrubs is not considered in the model. This upper level vegetation affects the thickness and density of the snow cover, along with the amount of solar radiation reaching the ground surface. The model takes into account only low-level vegetation (surface vegetation) that is less than 0.5 meter high, because the information about higher vegetation such as trees and tall shrubs is already incorporated into the monthly surface air temperature data, which were used as input data in the model.

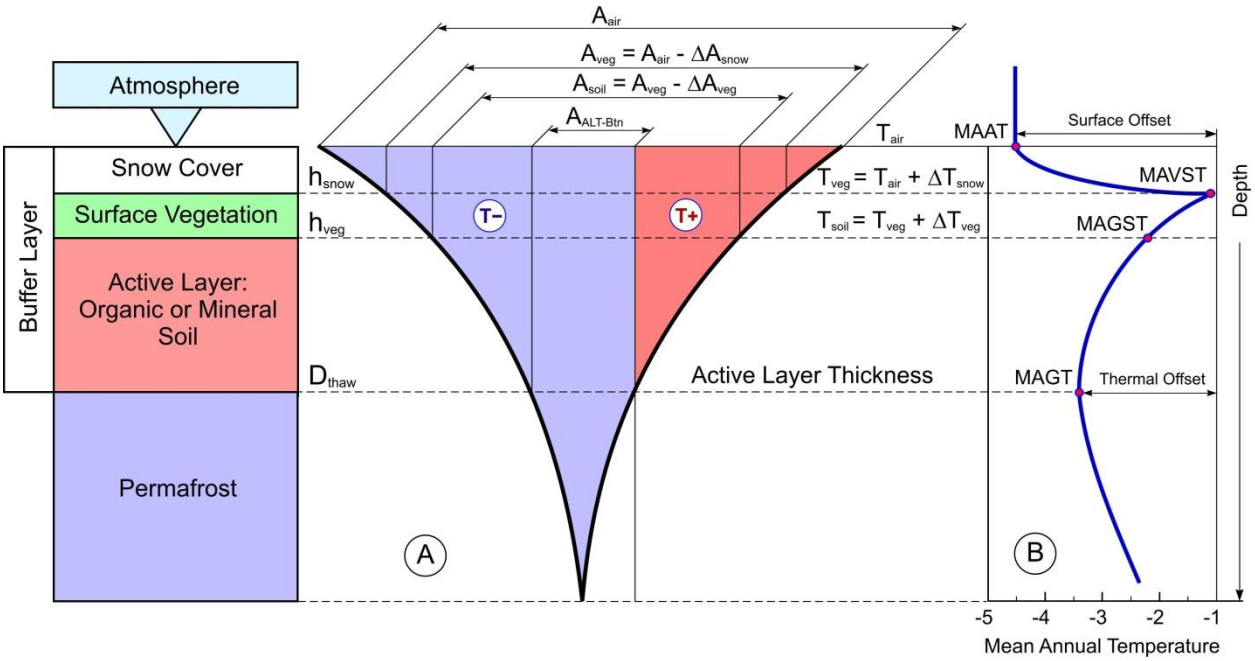

Figure B1. The GIPL 1.0 model conceptual diagram (A) and schematic profile of mean annual temperature through the lower atmosphere, active layer and upper permafrost (B). Acronyms: MAAT (Mean Annual Air Temperature), MAGST (Mean Annual Ground Surface Temperature), MAGT (Mean Annual Ground Temperature), ALT (Active-Layer Thickness).

Snow cover plays an important role in heat exchange processes between the surface of the ground and the atmosphere. The warming effect of the snow cover has been calculated using approximate formulas derived by A. Lachenbruch (1959) and V. Romanovsky (1987), which incorporate ground properties, vegetation cover, and their respective effect on heat turnovers through the snow. Heat turnovers are defined as the quantity of incident heat (during the heating period), or out-going heat (during the cooling period) throughout the media over a given time interval (usually half year increments). Thus, the heat turnover is $Q = \int_{t_1}^{t_2} q(t)dt$, where t_1 and t_2 are the times when the regime changes from ground heating to ground cooling, or from cooling to heating periods, and *q(t)* is the heat flux through the ground surface as a function of time.

Our model takes into account only conductive heat transfer through the surface vegetation (lichens, moss, and grasses). The rate of heat turnover between the ground and atmosphere has been shown to have a strong dependence on vegetation cover. In summer, surface vegetation prevents solar radiation from penetrating into the ground and warming it. In wintertime, surface vegetation acts as an insulator and keeps heat in the ground.

The seasonal freezing and thawing cycles cause changes in the thermal properties of soils within the active layer. Typically, this effect leads to a decrease in MAGTs with depth within the active layer. The thermal offset is defined as the difference between the mean annual temperature MAGT at the bottom of the active layer and the mean annual temperature at the ground surface (Kudryavtsev et al. 1974, Goodrich 1978, Burn and Smith 1988). The thermal offset depends on soil moisture content

and thermal properties, and has the most pronounced effect within a peat layer (Marchenko and Romanovsky 2007). The analytical equation to estimate the thermal offset was given by Kudryavtsev (1981) (no derivation was published), and was formally derived by V. Romanovsky (Romanovsky and Osterkamp 1995).

The approach to simulate MAGT in the GIPL 1.0 model is the consecutive layer-by-layer introduction of thermal effects of snow, ground surface vegetation, and the soils within the active layer on mean annual temperatures and seasonal amplitudes at each considered level (snow surface, vegetation surface, and ground and permafrost table). However, this scheme is not totally additive because the estimation of the impact of each new layer already includes the thermal effects of all layers above it. Moreover, in this approach, the thermal effect of snow reflects the thermal properties and temperature field dynamics in the subsurface layers through the heat turnover estimation. As a result, this approach takes into account some negative and positive feedbacks between designated layers in the "atmosphere-permafrost" system.

The Active-Layer Thickness

Calculation of the ALT is the final step in the GIPL 1.0 model (Romanovsky and Osterkamp 1997). The formula was derived for homogeneous ground, but in actuality, even if the soil properties are the same throughout the active layer, the moisture content or mode of heat flow may vary significantly. This can make the active layer inhomogeneous with regard to its thermal properties. Also, the model does not take into account unfrozen water, which can exist in the frozen active layer even at temperatures below zero Celsius, and has a significant effect on the ground's thermal properties (Williams 1964, Williams and Smith 1989). The assumption of a periodically steady state temperature regime seems to be a good approximation when applied to the annual temperature cycle, which varies from year to year (Romanovsky and Osterkamp 1997). Considering the advantages along with the shortcomings, the GIPL 1.0 model appears to give a good representation of the coupling between permafrost and the atmosphere. When applied to long-term (decadal and longer time scale) averages, this approach shows an accuracy of +0.2-0.4ºC for the mean annual ground temperatures and +0.1 – 0.3 m for the active-layer thickness calculations (Sazonova and Romanovsky 2003). The relative errors do not exceed 32% for the ALT calculations, but typically they are between 10 and 25%. The differences in 0.2-0.4°C between calculated and measured mean annual ground temperatures were obtained for the long-term multi-year average estimations.

The Input Dataset

At the present stage of development, the GIPL 1.0 model is combined with ArcGIS to facilitate preparation of input parameters (climate forcing from observations or from Global or Regional Climate Models) and visualization of simulated results in a form of digital maps (Figure B2).

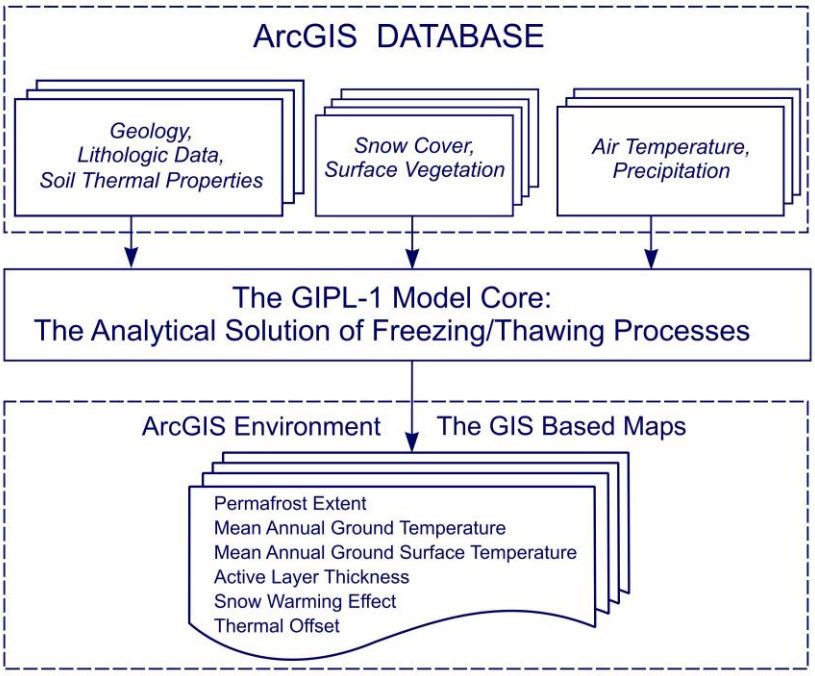

Figure B2. The GIS merged GIPL-1 schematic diagram.

Literature Cited

Brown, J., and R. A. Kreig. 1983. Guidebook to permafrost and related features along the Elliot and Dalton highways, Fox to Prudhoe Bay, Alaska. Proceedings of Fourth International Conference on Permafrost. 18–22 July 1983, University of Alaska, Fairbanks, Alaska Division of Geological and Geophysical Surveys, 230 pp.

Burn, C. R., and C. A. S. Smith. 1988. Observations of the 'thermal offset' in near-surface MAGTs at several sites near Mayo, Yukon Territory, Canada. Arctic 41(2):99–104.

Feldman, G. M., A. S. Tetelbaum, N. I. Shender, and R. I. Gavriliev. 1988. The guidebook for temperature regime forecast in Yakutia (in Russian), Yakutsk, 240 pp.

Goodrich, L. E. 1978. Some results of numerical study of ground thermal regime. Proceedings of the Third International Conference on Permafrost. National Research Council of Canada, Ottawa, vol.1:29–34.

Kudryavtsev, V. A. (editor). 1981. Permafrost (short edition) (in Russian), MSU Press, 240 pp.

Kudryavtsev, V. A., L. S. Garagula, K. A. Kondrat'yeva, and V. G. Melamed. 1974. Osnovy merzlotnogo prognoza (in Russian). MGU Press, 431 pp. [CRREL Translation: V. A. Kudryavtsev et al. 1977. Fundamentals of frost forecasting in geological engineering investigations, CRREL Draft Translation 606, 489 pp.]

Lachenbruch, A. H. 1959. Periodic heat flow in a stratified medium with application to permafrost problems. US Geological Survey Bulletin, 1083-A, 36 pp.

Marchenko, S., and V. E. Romanovsky. 2007. Modeling the effect of organic layer and water content on permafrost dynamics in the northern hemisphere. Eos, Transactions, American Geophysical Unions, 88(52), Fall Meet. Suppl., GC23A-0985.

Romanovsky, V. E. 1987. Approximate calculation of the insulation effect of the snow cover. Geokriologicheskie Issledovania (in Russian), MGU Press, vol. 23, 145–157.

Romanovsky, V. E., and T. E. Osterkamp. 1995. Interannual variations of the thermal regime of the active layer and near-surface permafrost in Northern Alaska. Permafrost and Periglacial Processes 6(4):31–335.

Romanovsky, V. E., and T. E. Osterkamp. 1997. Thawing of the active layer on the coastal plain of the Alaskan Arctic. Permafrost and Periglacial Processes 8(1):1–22.

Sazonova, T. S., and V. E. Romanovsky. 2003. A model for regional-scale estimation of temporal and spatial variability of active layer thickness and mean annual ground temperatures. Permafrost and Periglacial Processes 14:125–139.

Williams, P. J. 1964. Unfrozen water content of frozen soils and soil moisture suction. Geotechnique 14(3):231–246.

The Department of the Interior protects and manages the nation's natural resources and cultural heritage; provides scientific and other information about those resources; and honors its special responsibilities to American Indians, Alaska Natives, and affiliated Island Communities.

NPS 190/124322, April 2014

National Park Service
U.S. Department of the Interior

Natural Resource Stewardship and Science
1201 Oakridge Drive, Suite 150
Fort Collins, CO 80525

www.nature.nps.gov